

Mud volcanoes and dissolution structures as kinematic markers during salt tectonic deformation

Chris Kirkham | Joe Cartwright

Department of Earth Sciences, University of Oxford, Oxford, UK

Correspondence

Chris Kirkham, Department of Earth Sciences, University of Oxford, South Parks Road, Oxford OX1 3AN, UK.
Email: christopher.kirkham@earth.ox.ac.uk

Abstract

The recognition of linear trails of fluid escape pipes that have been deformed by salt flow have recently been suggested to offer a novel approach to reconstructing the internal kinematics of thick salt sequences deforming under gravity. These deformed pipes constrain a number of key parameters for salt tectonic analysis including the salt flow direction, translation distance of the top salt and overburden, the internal flow profile and from the flow velocity, the bulk viscosity of the salt. Here we interpret and characterise two previously unrecognised large-scale strain markers within a salt sequence that may be equally as valuable as the deformed pipes for constraining salt flow. This study is based on the interpretation of a ca. 4,600 km² 3D seismic survey from the outer slope of the Nile Cone, offshore Egypt, located at the boundary between the extensional and translational domains of the deformed marginal region of the Messinian salt basin. We mapped five deformed pipe trails that allow us to constrain the average flow velocity of the top salt, at ca. 2 mm/yr over the past 2–3 Myrs. The salt flowed in a basinward NW/NNW direction away from the basin margin. In addition, we mapped two large (ca. 2 km diameter) salt dissolution depressions formed by subjacent dissolution of the evaporites. These are presently located down the salt flow direction of a large remnant erosional high at the base of the salt, and in the general alignment of one of the pipe trails. We therefore argue that this dissolution structure most likely formed by fluid venting from the base salt high, and as such can be used to measure translation direction, distance and average velocity. The second of the two novel kinematic indicators requires mapping of genetically connected mud volcanoes and their depletion zones. The study area contains over 400 individual mud volcanoes that are sourced from beneath the salt and erupted from the Early Pliocene to Recent. A subset of these, extruded at or near to the present day seafloor, have well imaged pre-salt depletion zones vertically beneath the erupted volcanic cones. A smaller subset, typically buried Early Pliocene extrusions, is found to have volcanic cones that are systematically offset laterally from their corresponding depletion zones, with an offset direction

This is an open access article under the terms of the Creative Commons Attribution License, which permits use, distribution and reproduction in any medium, provided the original work is properly cited.

© 2021 The Authors. *Basin Research* published by International Association of Sedimentologists and European Association of Geoscientists and Engineers and John Wiley & Sons Ltd.

and distances closely matched with other kinematic markers. Hence we suggest that mud volcanic plumbing systems can provide another independent kinematic marker from which to infer salt flow regime.

KEYWORDS

dissolution structure, Eastern Mediterranean, fluid escape pipes, kinematic markers, Messinian Evaporites, mud volcanoes, salt tectonics, sedimentary basin

1 | INTRODUCTION

Many sedimentary basins on Earth are underlain by thick and regionally extensive salt sequences (see table 2.4 in Jackson & Hudec, 2017) that flow and deform over geological time driven by some combination of differential loading, basin tilting through uplift/subsidence or regional plate kinematics (Brun & Fort, 2011; Gemmer et al., 2004; Peel, 2014). The flow of salt and associated deformation of its overburden has a substantial impact on the structural architecture of many sedimentary, rift and foreland basins (Davison et al., 2012; Quirk et al., 2012; Rowan et al., 2004; Stewart, 2007). The nature of this deformation is heavily influenced by the direction and internal flow regime (e.g. Poiseuille, Couette or Squeeze flow profiles, or some combination of the three; see figure 8.1 in Jackson & Hudec, 2017) of the flowing salt layer, which is governed by the regional drivers for salt flow (Albertz & Ings, 2012; Gemmer et al., 2004; Quirk et al., 2012). A major goal of salt tectonics is therefore to understand the evolving kinematics of a flowing layer of salt and to use the kinematic constraints to infer the driving mechanisms governing the deformation.

Despite the importance of understanding the flow regime in salt, direct measurements of the internal kinematics in flowing salt layers has proved challenging to obtain. In their absence, our understanding of the flow regime and especially its relationship to different drivers has been based on numerical and physical models (Albertz & Ings, 2012; Davison et al., 1996; Dooley et al., 2007; Gemmer et al., 2005; Li et al., 2012). In parallel to these modelling studies, interpretations made from seismic reflection data have provided some constraints of internal strain (Cartwright et al., 2012; Feng et al., 2017) and translation distances (Peel, 2014; Pichel et al., 2018).

More recently, Cartwright et al. (2018) identified deformed fluid escape pipes that transect the thick salt offshore Lebanon and used them to provide the first direct calibration of the flow in a salt sequence. Cartwright et al. (2018) documented a linear trail of 21 fluid escape pipes with pockmarks at their outlets, which all rooted to the crest of a major pre-salt anticline named Oceanus. The stratigraphic position of the pockmarks records the timing

Highlights

- Structures with genetically connected pre- and post-salt components present kinematic markers for flowing salt.
- Mud volcano systems and salt dissolution structures represent novel kinematic markers.
- These kinematic markers reveal a unidirectional salt flow consistent with the marginal fault system.
- The onset of salt flow was diachronous along the basin margin.
- A Couette flow profile is the simplest explanation for the observed translation of the overburden.

of fluid expulsion (Cartwright & Santamarina, 2015). These pockmarks record the successive episodes of expulsion from ca. 1.7 Ma to Recent and are linearly distributed (NW-SE), with the youngest positioned directly above the crest of the pre-salt fold and an increase in pockmark age towards the NW in the basinward salt flow direction. Translation of the overburden above the basinward flowing salt offset the pockmarks from their originally formed location above the crest of the pre-salt anticline. The outermost pipe in the trail was interpreted to have been deformed in the salt into an approximate Couette flow profile geometry (see figures 2 and 3 in Cartwright et al., 2018).

The methodology developed by Cartwright et al. (2018) has since been further validated (Kirkham et al., 2019) and more linear pipe trails have been interpreted around the Levant Basin (Oppo et al., 2020). The interpretation of these natural kinematic markers from the Levant Basin has opened a new approach to salt kinematics, providing constraints for flow regime, velocity and direction of salt flow. However, deformed fluid escape pipes may only have quite specific distribution in some, but not all salt basins, which leads us to consider whether we can identify other and perhaps more widely occurring natural

strain markers for the internal kinematics of a flowing salt layer. A strain marker should be a geological feature that would be displaced and/or deformed by the flow of a salt layer.

Mud volcanoes are widely distributed and commonly observed within the evaporitic subbasins of the Eastern Mediterranean and their plumbing systems often root beneath the salt, with surface extrusions above the salt (Dupré et al., 2014; Huguen et al., 2009; Kirkham et al., 2017; Loncke et al., 2004; Mascle et al., 2014; Prinzhofer & Deville, 2013). The most prolific of these mud volcano provinces is found in the outer shelf slope of the western Nile where >400 mud volcanoes sourced from beneath the salt have been extruded at seabeds over the past 5 Myrs (Kirkham et al., 2017; Figure 1). This mud volcano province lies within an area of salt-lubricated gravity tectonics at the southern margin of the main salt basin (Loncke et al., 2006). Kirkham et al. (2018b) identified vertical pipe-like conduits that cross-cut the thick Messinian Evaporite seal and whose seismic character and geometry are directly analogous to fluid escape pipes (Cartwright & Santamarina, 2015; Løseth et al., 2011). These conduits connect the mud edifices to bowl-shaped depletion zones in the Pre Salt (Kirkham et al., 2017) that formed by the withdrawal of mobilised mud (Dupuis et al., 2019; Stewart & Davies, 2006). The mud edifices and their depletion zones are separated by the full thickness of a flowing salt sequence. The combination of mud edifices, conduits and depletion zones (the mud volcano

plumbing system) therefore constitute a potential strain marker for the salt.

The main aim of this study was to evaluate whether the mud volcanic plumbing system can indeed be used as a strain marker for salt flow. A secondary aim is to explore if an additional category of strain marker can be considered, namely subsidence depressions related to localised salt dissolution. The study builds on a large body of existing work on this mud volcanic province (Dupré et al., 2014; Giresse et al., 2010; Huguen et al., 2009; Kirkham et al., 2017, 2018b; Loncke et al., 2004; Mascle et al., 2014; Pierre et al., 2014; Prinzhofer & Deville, 2013), and is facilitated by the availability of high fidelity 3D seismic data. The paper concludes with a discussion of the kinematic constraints obtained within the study area and their implications for the salt tectonic evolution of this basin margin.

2 | GEOLOGICAL SETTING

2.1 | Stratigraphic evolution of the Western Nile

The study area is located within the outer shelf slope of the western Nile Cone offshore Egypt at water depths of 2,500–3,000 m (Figure 1). Opening of the Gulf of Suez as well as tilting of northern Egypt during the Upper Eocene resulted in the introduction of large quantities of terrigenous clastics into the basin, which had been characterised primarily

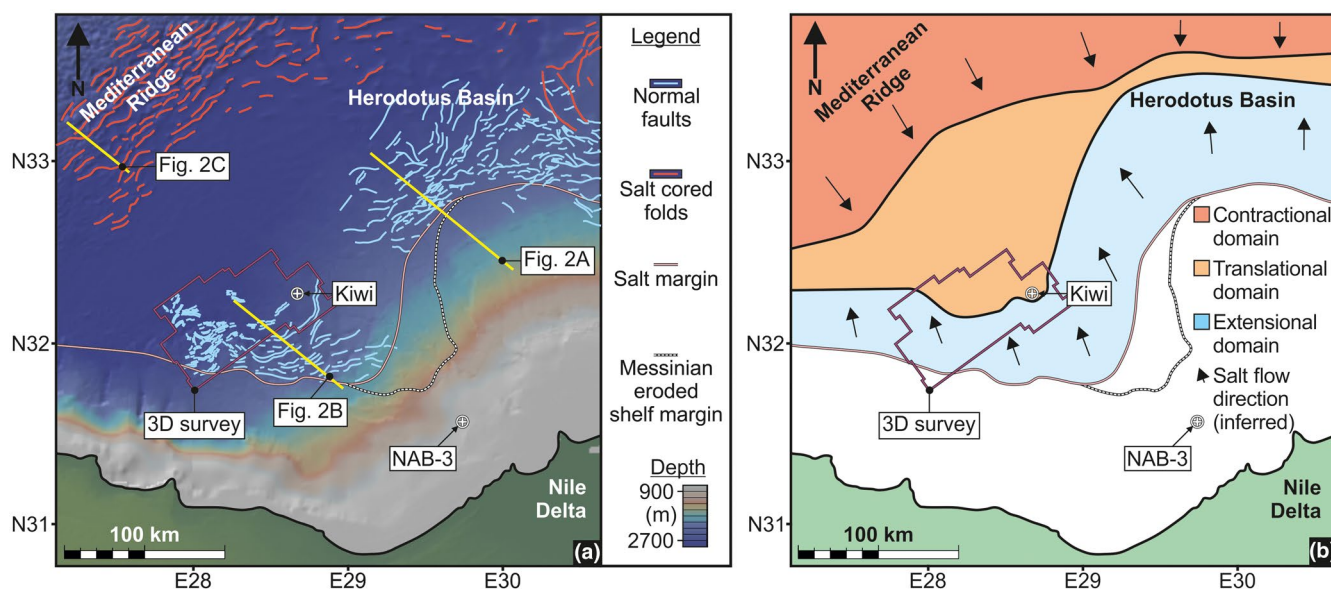


FIGURE 1 Geological setting and salt flow domains of the Western Nile province. (a) A bathymetric map (from GeoMapApp www.geomapapp.org) showing the main structural elements in the study area offshore the western Nile Delta (compiled from Allen et al., 2016; Loncke et al., 2006; Zucker et al., 2020 and new interpretation), as well as the location of the 3D seismic survey and Kiwi and NAB-3 exploration wells. Salt margin modified from Loncke et al. (2006) and Lofi et al. (2011). (b) A map of the study area showing the extensional, translational and contractional domains of the salt basin, as well as the salt flow direction inferred from normal faults and folds in Figure 1a

by carbonate deposition during the lower and mid-Eocene (Dolson et al., 2005; Said, 1962; Salem, 1976). From the upper Eocene and throughout the Oligocene and Miocene this basin was dominated by the deposition of clastic sediments (Barber, 1981; Said, 1962; Salem, 1976).

Clastic deposition was temporarily superseded in the Late Miocene by rapid deposition of a thick mobile evaporitic sequence (Figure 2) during the Messinian Salinity Crisis (ca. 5.97 to 5.33 Ma; Krijgsman et al., 1999; Manzi et al., 2013; Meilijson et al., 2019). Progressive disconnection of the Mediterranean Sea from the Atlantic Ocean and restriction of marine input (Flecker et al., 2015; Hsü et al., 1973) led to the accumulation of predominantly halite in the deep offshore basins that is typically 1–1.5 km thick. The Messinian Salinity Crisis terminated during the Zanclean reflooding when the Mediterranean and Atlantic Ocean were reconnected (Garcia-Castellanos et al., 2009). The basin was dominated by clastic deposition during the

Pliocene to Recent through the development of the Nile Delta and Nile Deep Sea Fan (NDSF; Loncke et al., 2006).

An exploration well (Kiwi-1) drilled in 2010 in the study area provides some limited lithological constraints on the pre-salt stratigraphy (Figures 1 and 3). Baer et al. (2016) reported that the Pre Salt consisted of thick sandstones interbedded with claystones in the Oligocene sequence, overlain by dominantly claystones, thin carbonates and thin sandstones in the Miocene sequence (Figure 3).

2.2 | Salt tectonics in the Western Nile

Gravity tectonics are an important feature of the geology of the study area. Widespread flow of the Messinian Evaporites during the Pliocene to Recent has led to the development of an extensional domain consisting of an array of margin-parallel normal faults detaching in the salt, a translational domain

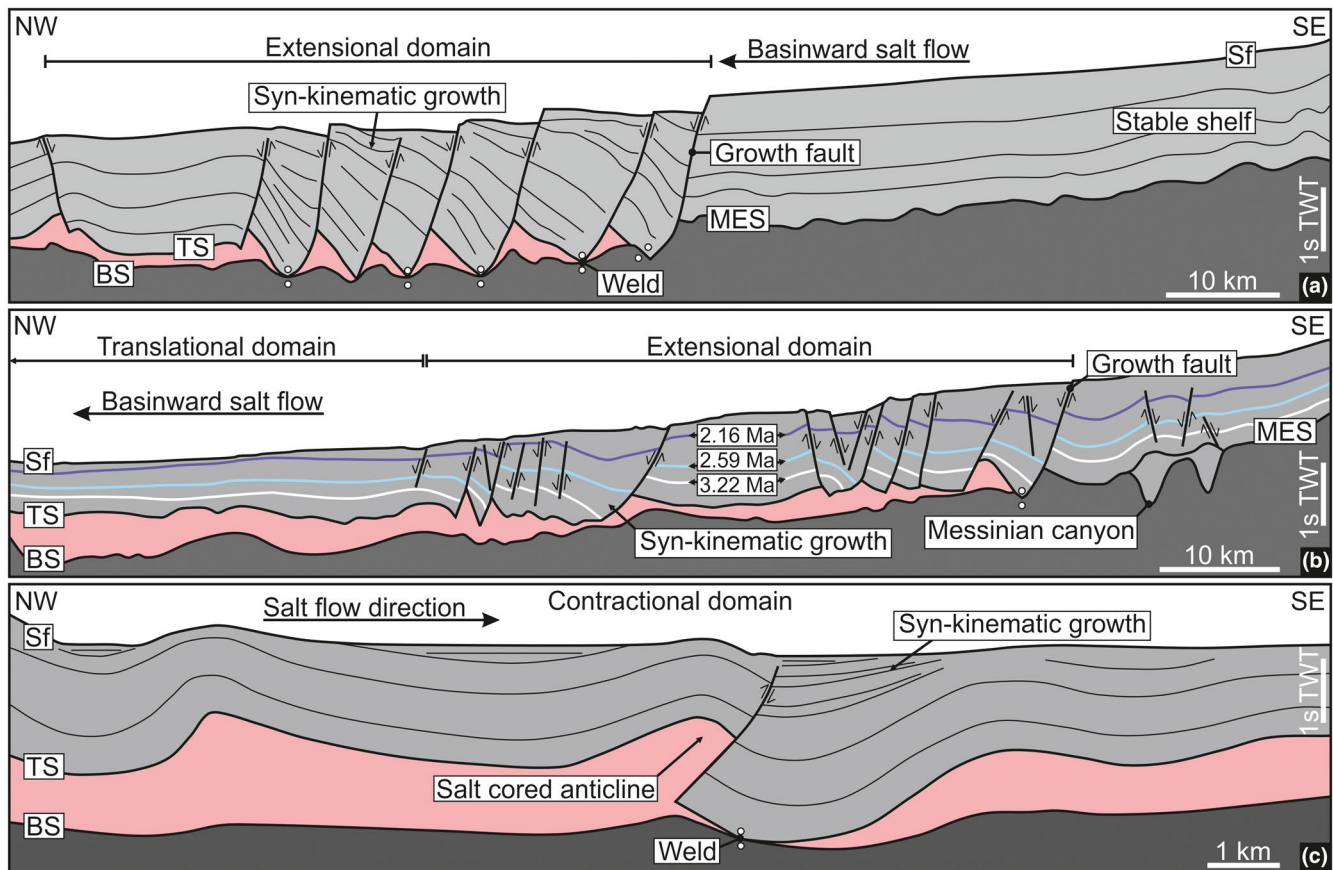


FIGURE 2 Regional cross sections through the study area (modified from Allen et al., 2016; see Figure 1a for locations). (a) A cross section through the extension domain, 90 km to the NE of the seismic survey area (Figure 1a), showing growth faults that have formed as a result of basinward salt flow and detach in the salt, sometimes resulting in a weld between the Pre Salt and Post Salt. (b) A cross section through the extensional and translational domains in the south of the study area showing dated key marker horizons (± 0.25 Myrs) and syn-kinematic growth in the hanging walls of normal faults. Note the absence of a thick prograding wedge over the salt from the Nile Delta (cf. Zucker et al., 2020). (c) A cross section through the contractual domain in the study area near the Mediterranean Ridge, showing salt cored anticlines verging SE and syn-kinematic growth packages. BS, Base Salt; MES, Messinian Erosional Surface; Sf, Seafloor; TS, Top Salt

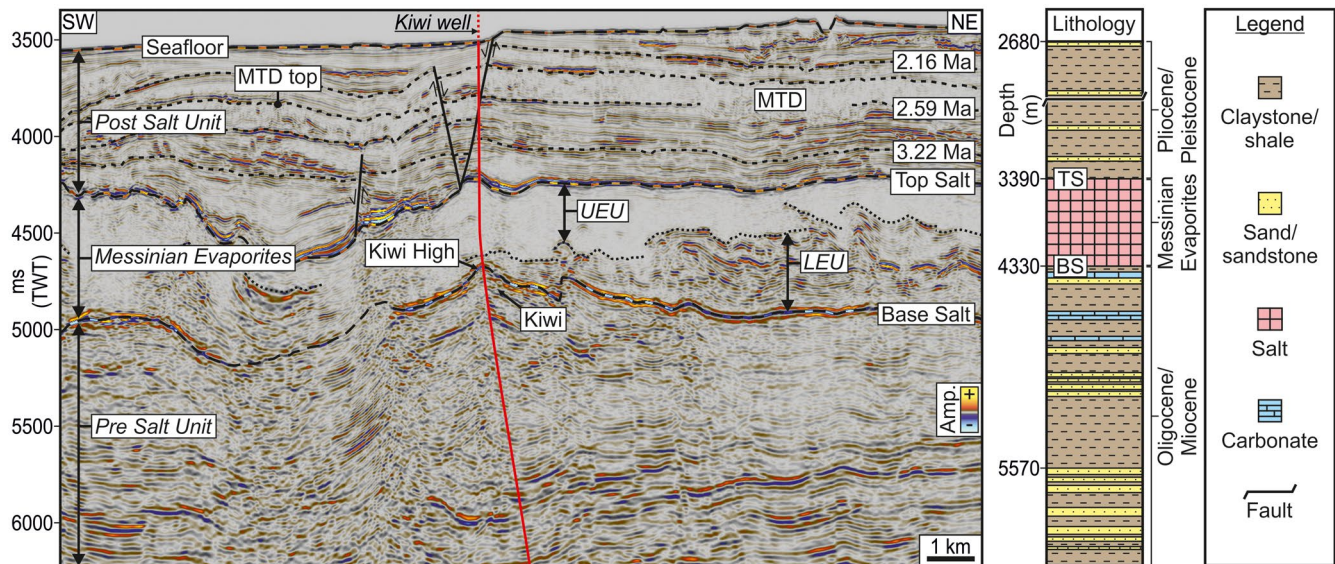


FIGURE 3 Seismic to proposed lithology tie at the Kiwi well (see Figures 1 and 4a for location; modified from Baer et al., 2016). The seismic profile shows the trajectory of the Kiwi well through the structure named Kiwi in the Pre Salt Unit. BS, Base Salt; LEU, Lower Evaporitic Unit; MTD, Mass transport deposit; TS, Top Salt; UEU, Upper Evaporitic Unit

characterised by an absence of larger structures, and a distal contractional domain consisting of salt-cored detachment folds and thrusts that also detach in the salt (Figures 1 and 2; Allen et al., 2016; Loncke et al., 2006). The outer region of the contractional domain coincides with a major basement involved thrust complex, the Mediterranean Ridge (Figure 1; Loncke et al., 2006), whose activity in the Pliocene to Recent almost certainly contributed a tectonically driven flow of salt to the southeast to oppose the downslope flow from the updip extensional domain. The dominant strikes of the structures in the extensional and contractional domains are broadly similar with modest scatter about a general NE–SW orientation (Figure 1), which supports the interpretation of a generally basinward, north-westerly flow of the salt linking these two domains. The study area straddles the outer part of the extensional domain, and the inner part of the translational domain (Figure 2b), so is ideally located to test these regional flow inferences derived from the gross structural zonation.

Differential gravitational loading of the Messinian Evaporites by the NDSF, resulting in ‘squeeze flow’, has historically been interpreted as the dominant driver for basinward salt flow in the environs of the NDSF, leading to a radial deformation pattern in the Pliocene to Recent overburden (Loncke et al., 2006). This interpretation has been challenged recently by Zucker et al. (2020) who argue that while sediment loading is the most likely driver on the eastern side of the NDSF, only the distal part of the NDSF wedge overlies the margin of the salt layer on its western side, where our study area is located. It is considered that sediment loading would have only exerted

a small influence in this area, with the dominant driver for salt flow most likely to be elevation head, leading to downslope gravity gliding of the entire salt-overburden sequence (Zucker et al., 2020).

3 | DATA AND METHODS

The data used in this study consist of a pre-stack time migrated (PSTM) and pre-stack depth migrated (PSDM) seismic survey, both covering the same ca. 4,300 km² area (Figure 4a). The binset dimensions of 12.5 × 6.25 m yield a lateral resolution of 25 m. The data have been processed to zero phase and displayed with SEG normal polarity (Brown, 2004), so that an increase in acoustic impedance downwards (an acoustically hard reflection) appears as a positive amplitude. Seismic interpretation was undertaken using Schlumberger’s Petrel software package. All horizons were manually picked and auto-correlated. Coherency and root-mean square (RMS) amplitude volumes were generated and interpreted in horizontal time-slices to recognise faults and fluid flow features including pipe-like conduits, pockmarks and mud volcanoes. These focused fluid flow features were identified (Figure 4a) following the methodologies set out by Cartwright and Santamarina (2015), Kirkham et al. (2017) and Kirkham et al. (2018b).

The seismic stratigraphy is divided here into the Pliocene to Recent (Post Salt), Messinian Evaporites; and the Oligo-Miocene (Pre Salt; Figure 4b). Description of the Pre Salt is restricted here to the Oligo-Miocene as this is a main focus for this study. Average P-wave velocities

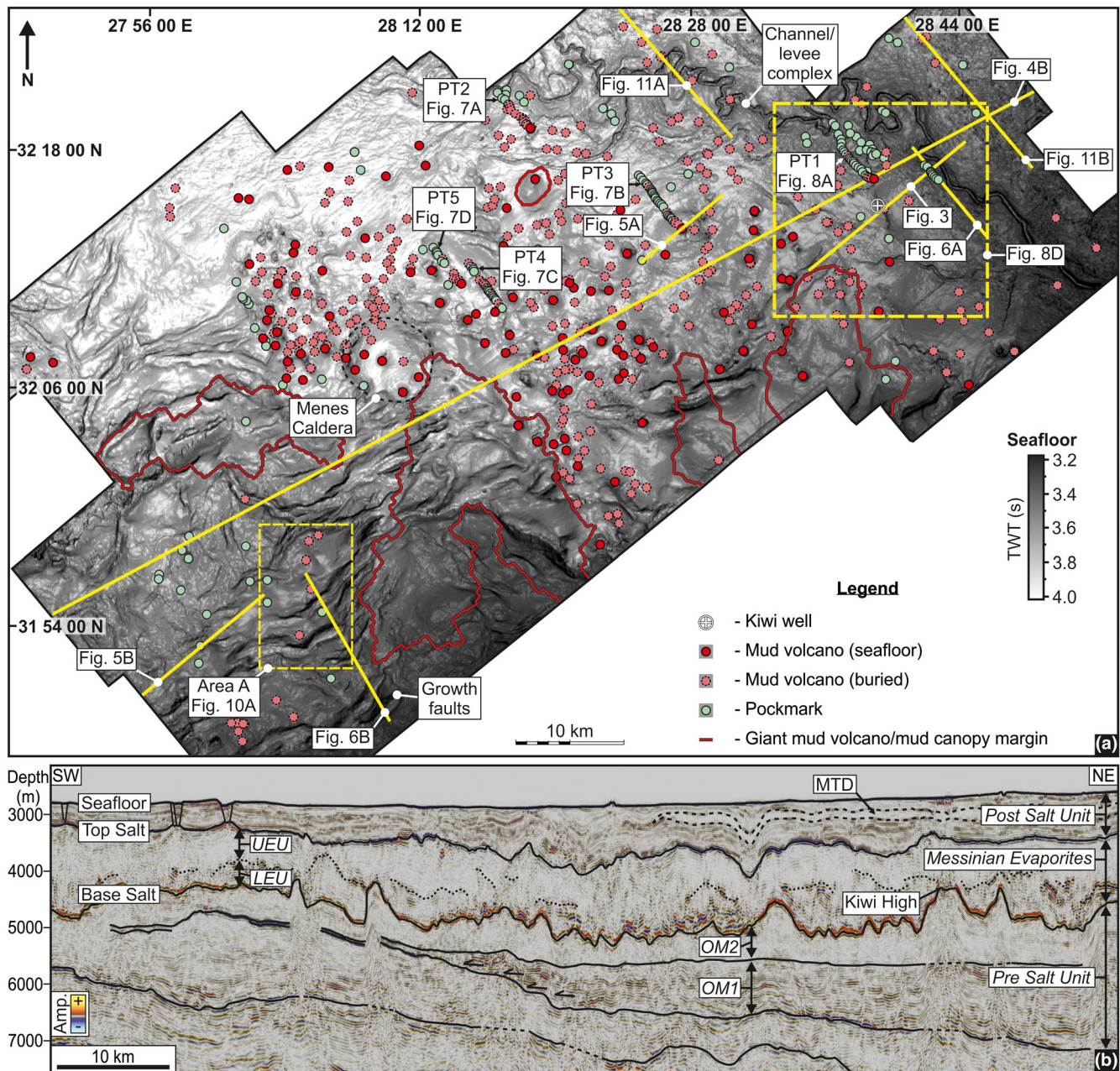


FIGURE 4 Mud volcanism, fluid escape and seismic stratigraphy in the study area. A: A seafloor map in the study area showing growth faults to the south, a channel/levee complex to the northeast, the Menes Caldera depression centrally (Dupré et al., 2014; Huguen et al., 2009) and the distribution of pockmarks and mud volcanoes. The location of five linear pipe trails (PT1-PT5) are highlighted. B: A seismic cross section through the entire 3D seismic survey (see Figure 4a for line location), highlighting key marker horizons and seismic stratigraphic units. LEU, Lower Evaporitic Unit; MTD, Mass transport deposit; OM1, Oligo-Miocene 1; OM2, Oligo-Miocene 2; UEU, Upper Evaporitic Unit

through these units, obtained from comparison of the PSTM and PSDM seismic surveys, are 1,800, 4,400 and 2,200 m/s respectively. Age calibration of the Pliocene to Recent interval was critical for dating pockmarks, mud volcanoes and salt dissolution structures. This was obtained by correlating three key seismic markers (3.22, 2.59 & 2.16 Ma; Figure 2b) from the NAB-3 exploration well (Gulmammadov, 2017) to our 3D seismic survey

(Figure 1). These key marker horizons have cumulative errors in dating of ± 0.25 Myrs (sum of biostratigraphic age dating and seismic correlation errors). Average sedimentation rates (uncorrected for compaction) between the dated markers were used to estimate ages of intervening seismic horizons. Estimates based on this latter approach are identified as such in the presentation of the results, and carry larger uncertainty values.

4 | RESULTS

4.1 | Seismic stratigraphy

4.1.1 | Pre Salt Unit (Oligo-Miocene)

The Pre Salt Unit has a wedge shaped geometry, increasing in thickness northwards from 80 to 2,900 m. The Pre Salt Unit is subdivided here into two subunits, Oligo-Miocene 1 (OM1) and Oligo-Miocene 2 (OM2; Figure 4b), based primarily on gross reflection amplitude and stratal reflection geometry. The OM1 is the deeper of the two subunits and is characterised by moderate to high amplitude reflections with good lateral continuity. These reflections onlap or condense onto a laterally continuous high amplitude, hard reflection defining the base of OM1 (Figure 4b). The hard reflection is interpreted to mark the abrupt contact with the underlying Eocene carbonate platform succession (Dolson et al., 2005). OM1 contains numerous channelised units and lobes and most likely represents a slope fan complex consisting of reservoir prone sandstone layers and interbedded claystones (Figure 3).

OM2 is characterised by a low amplitude discontinuous reflections, with an upper boundary at the Base Salt (Figure 4b). OM2 is parallel stratified over the greater part of the study area, but is irregularly preserved due to erosion at the Base Salt and by the formation of depletion zones for the many mud volcanoes erupted during the Pliocene to Recent (Figures 4b and 5). The removal of sediment from OM2 by the process of mud depletion resulted in the development of 100s of circular to elliptical depressions at the Base Salt and distortion of reflection configurations in OM2 on the flanks

of the depressions (Figure 5a). The Top Salt is almost invariably deformed concordantly with the Base Salt above each of these depletion zones (Kirkham, 2016; Kirkham et al., 2017). Individual depletion zones often amalgamate in areas of particularly dense mud volcano formation, producing regions of complex Base Salt topography that have an irregular 'egg box' geometry (Kirkham et al., 2017).

4.1.2 | Messinian Evaporites

The Messinian Evaporites reach thicknesses >2 km in the deep basin and thin to a pinch out or weld towards the Nile Delta and Egyptian continental margin (Figures 1 and 2). They can be sub-divided into upper and lower seismic units (Figures 4b and 6a), referred to here as the Upper Evaporitic Unit and the Lower Evaporitic Unit respectively. The Lower Evaporitic Unit is characterised by moderate to high amplitude, discontinuous reflections interbedded with seismically transparent layers (Figure 6a). The Upper Evaporitic Unit is, in contrast, seismically opaque (Figure 6a), and is interpreted as being almost entirely composed of halite. The contrast in reflectivity of these upper and lower units is attributed to the interbedding of thin clastic units in the Lower Evaporitic Unit (Kirkham, Bertoni, et al., 2020). Long-range correlation of this unit suggests it is the lateral equivalent of the highly reflective series of Messinian evaporitic units (ME I–V) in the Levant Basin (see Figure 3 & Figure S2 in Kirkham, Bertoni, et al., 2020), where the reflectivity is due to just a few percent by gross thickness of sparsely bedded, thin (1–3 m thick) layers of diatomaceous claystone (Feng et al., 2017; Meilijson

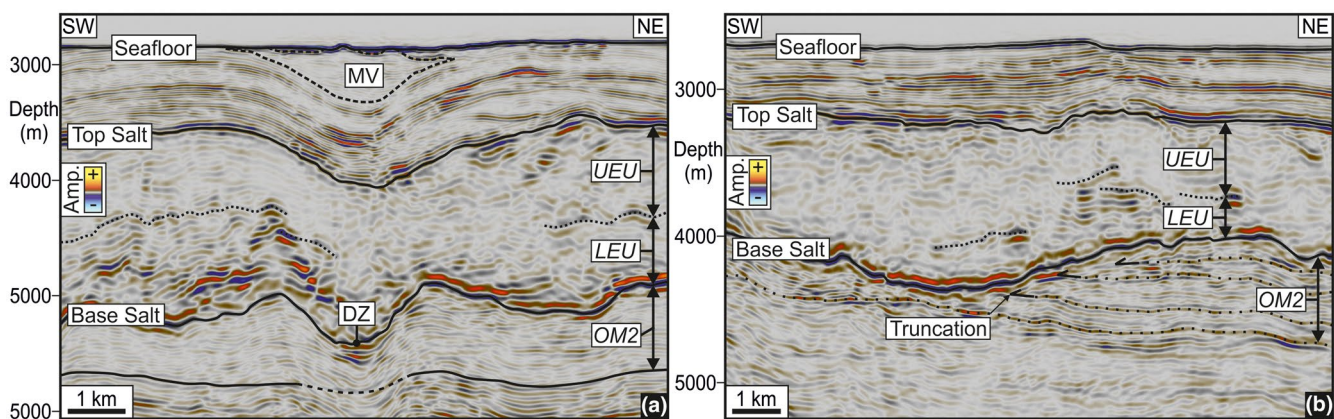


FIGURE 5 Anomalous base salt depressions and thinning of the Pre Salt Unit. Mud depletion vs. erosion (see Figure 4a for line locations). (a) A seismic cross section showing a mud volcano (MV) in the Post Salt Unit that is underlain by a bowl shaped depression at the Top Salt and Base Salt and thinning of the OM2 in the Pre Salt Unit that highlights a depletion zone (DZ). (b) An erosional depression at the Base Salt, thinning and truncation of parallel reflections within the OM2 against the depression and discordance of the Top Salt and Base Salt. LEU, Lower Evaporitic Unit; OM2, Oligo-Miocene 2; UEU, Upper Evaporitic Unit

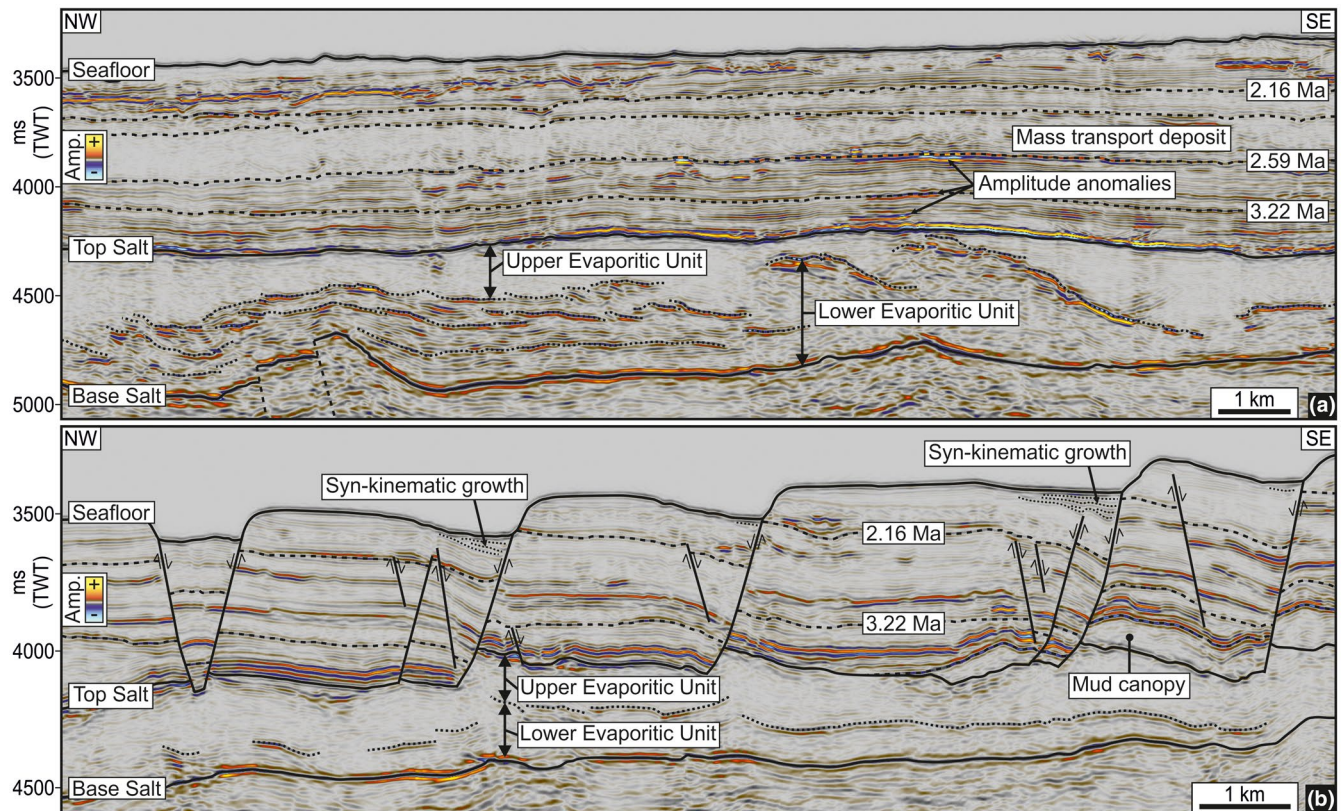


FIGURE 6 Seismic stratigraphy and structure of the Messinian Evaporites and growth faults in the Post Salt Unit (see Figure 4a for line locations). (a) The Messinian Evaporites are divided here into the transparent Upper Evaporitic Unit and the moderate-high amplitude Lower Evaporitic Unit. The Lower Evaporitic Unit shows significant isopach variation and reveals internal deformation in the salt formed by its flow. (b) Growth faults in the Post Salt Unit, in the southwest of the study area, that detach in the Messinian Evaporites and record minor syn-kinematic growth in the Late Pleistocene-Holocene

et al., 2019). Welding of the entire Messinian Evaporite succession to a single seismic loop is seen in the centre of the study area (Huguen et al., 2009; Kirkham, 2016; Kirkham et al., 2017). This suggests that the non-mobile/clastic sediment fraction within the Lower Evaporite Unit is indeed minimal, or at any rate too thin and too weak to constitute any significant internal mechanical obstruction to salt flow.

4.1.3 | Post Salt Unit (Pliocene-Recent)

The Post Salt Unit has a grossly wedged shape geometry in the study area (Figure 4b) decreasing in thickness basinward, away from the sediment output of the Nile Delta. The variable amplitude, laterally continuous, parallel stratified seismic facies of this unit is typical of hemipelagites (Figures 4b and 6a). These stratigraphically continuous hemipelagites are disrupted by a 100–200-m-thick mass transport deposit in the east of the study area (Figures 3 and 4b). This is interpreted to be the distal portion of a much larger slope failure (SL2 of Garziglia et al., 2008),

whose head scarp is located in the Rosetta Canyon over 100 km to the ESE.

The Post Salt Unit is largely undeformed by active faulting or folding over most of the study area, as would be expected in a largely translational domain. The southern region of the study area extends into the extensional domain (Figure 1b; Loncke et al., 2004, 2006), and this is expressed in an array of linear to curvilinear striking, listric normal faults that detach in the underlying Messinian Evaporites (Figures 4 and 6b). The maximum throw on these faults ranges from 40 to 250 m with heaves of 60–400 m (Figure 6b). They strike NE–SE to E–W parallel to the margins of the salt basin with lengths of 3–16 km. Many of these faults have scarps at the present day seafloor with relief of 25–150 m. Syn-sedimentary growth on these faults is interpreted from expansion indices to have initiated in the Late Pleistocene (Figure 6b). This onset date contrasts markedly with growth onsets on normal faults further to the east along the extensional domain, which initiated in the Early Pliocene, albeit with the most significant growth phase recorded over the last 3.22 Ma (± 0.25 Myrs; Figure 2b).

4.2 | Mud volcanism and fluid escape features

4.2.1 | Mud volcanism

North of the extensional domain, the central and northern sections of the study area are relatively undeformed but are a locus for >400 mud volcanoes extruded from the Early Pliocene to Recent (Kirkham et al., 2017; Figure 4a). The timing of formation of the mud volcanoes is determined by interpreting the age of the palaeo-seafloor reflection onto which each one was extruded. The mud volcanoes (Figure 5a) are easily identifiable as circular to elliptical, lenticular bodies with a grossly conical or inverted conical 3D geometry, with diameters ranging from 550 to 5,660 m, thicknesses of 25–510 m and volumes from 0.1 to 3.3 km³ (Kirkham et al., 2017).

The conduits feeding the mud volcanoes are visible for the most recently erupted mud volcanoes as vertical to sub-vertical pipe-like structures. Seismically, they are expressed as zones of abrupt reflection termination and low reflection coherence that transect the entire Messinian Evaporite

succession and are located directly beneath the central axis of each mud volcano (Kirkham et al., 2018b; Figure 7). These seismically visible conduits root at depth into the depletion zones of the Pre Salt Unit OM2 (Figure 5a).

Much larger volumes (up to 116 km³) of extruded mud sourced from OM2 were erupted onto the Top Salt surface at the end of the Messinian Salinity Crisis in the south of the study area (Figure 4b). These giant mud volcanoes cover areas of up to 300 km², reach up to 1 km in thickness and are fed by elongate (1–5 km long) conduits that cross cut the Messinian Evaporites (Kirkham et al., 2018a, 2020).

4.2.2 | Fluid escape pipes

Over 100 fluid escape pipes are widely distributed throughout the study area (Figure 4a). Their seismic expression is comparable to that of fluid escape pipes in many other basins (Cartwright & Santamarina, 2015) and interestingly, is also identical to that of the mud volcano conduits in this study area. However, instead of terminating upwards in

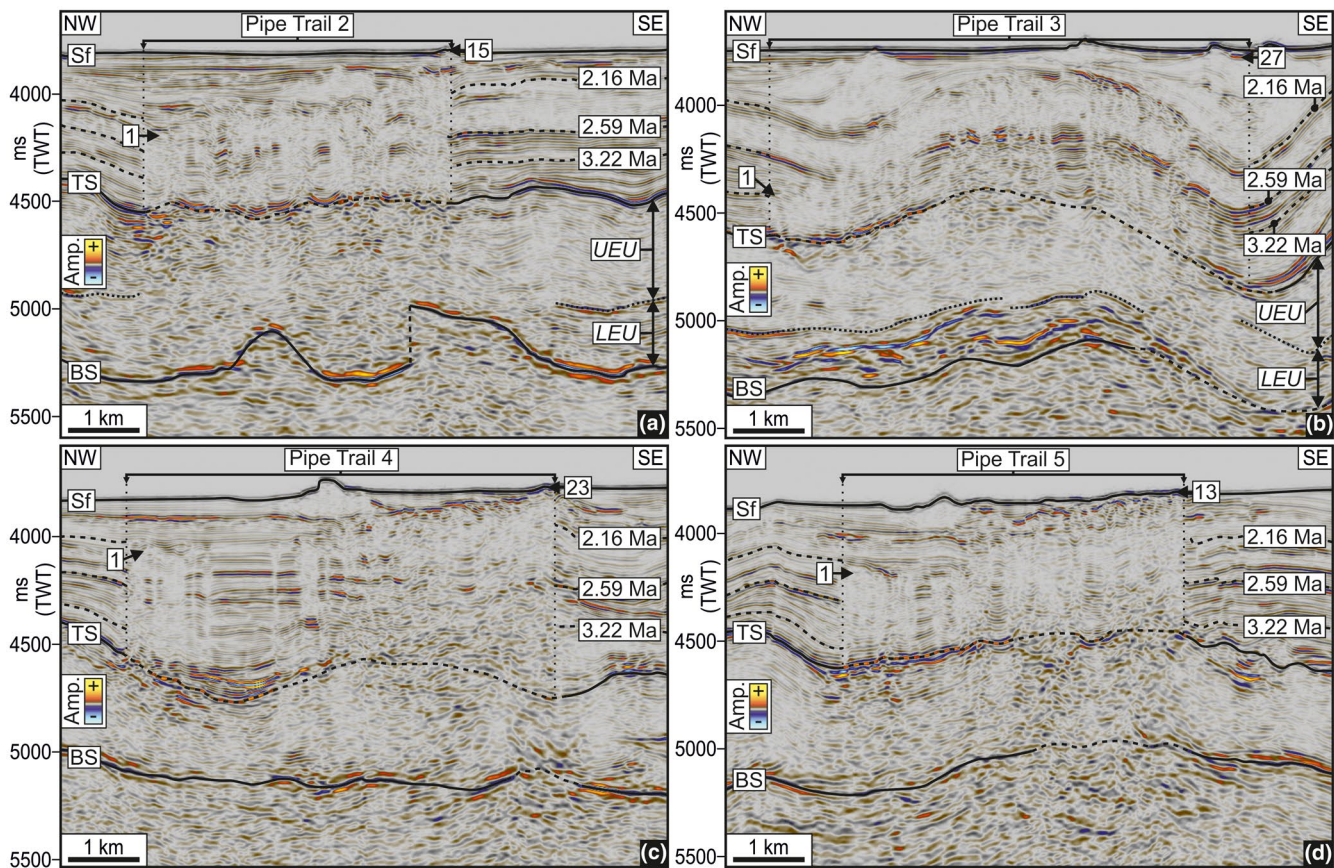


FIGURE 7 Linear trails of pipes with pockmarks and mud cones at their outlets. A-D: Seismic cross sections through Pipe Trails 2–5 (see Figure 4a for locations) with either pockmarks or mud cones at their outlets. The outlets are distributed in a NW-SE orientation through the Post Salt Unit, located at progressively deeper horizons toward the northwest and the most south-easterly outlet in each linear trail is positioned at the seafloor. The oldest (1) and most recent (e.g. 15 in Figure 7a) outlet in each linear trail is labelled. BS, Base Salt; LEU, Lower Evaporitic Unit; Sf, Seafloor; TP, Top Pliocene; TS, Top Salt; UEU, Upper Evaporitic Unit

an edifice, the fluid escape pipes terminate at large pockmark craters. The pockmark dimensions range from 70 to 500 m across, and 10–50 m of concave relief. The age of these pockmarks ranges from Late Pliocene to Recent.

The fluid escape pipes transect the Messinian Evaporites but cannot be traced any deeper. The vast majority emanate from local highs mapped at the Base Salt, as opposed to the roots of the mud volcano conduits that terminate downwards into depletion zone depressions of the Base Salt (Figures 7 and 8a,c). Going forward, we refer to fluid escape pipes and mud volcano conduits as pipes due to their analogous seismic character and geometry.

Of particular interest here are five clusters of pipes found in the central and north-eastern regions of the study area

(Figure 4a). These stand out from the more dispersed distribution of pipes in that they are strongly linearly aligned in planform. Closer inspection shows that these five linear clusters bare all the diagnostic characters of pipe trails sourced from a single focal point of fluid escape (cf. Cartwright et al., 2018). These five trails thus represent ideal kinematic markers for analysis of the salt flow regime (Kirkham et al., 2019; Oppo et al., 2020), and are described in detail below.

4.3 | Pipe trails as kinematic markers

The five pipe trails (labelled PT1-5; Figure 4a) are all linear in planform and oriented NW-SE (320° – 324°). The age

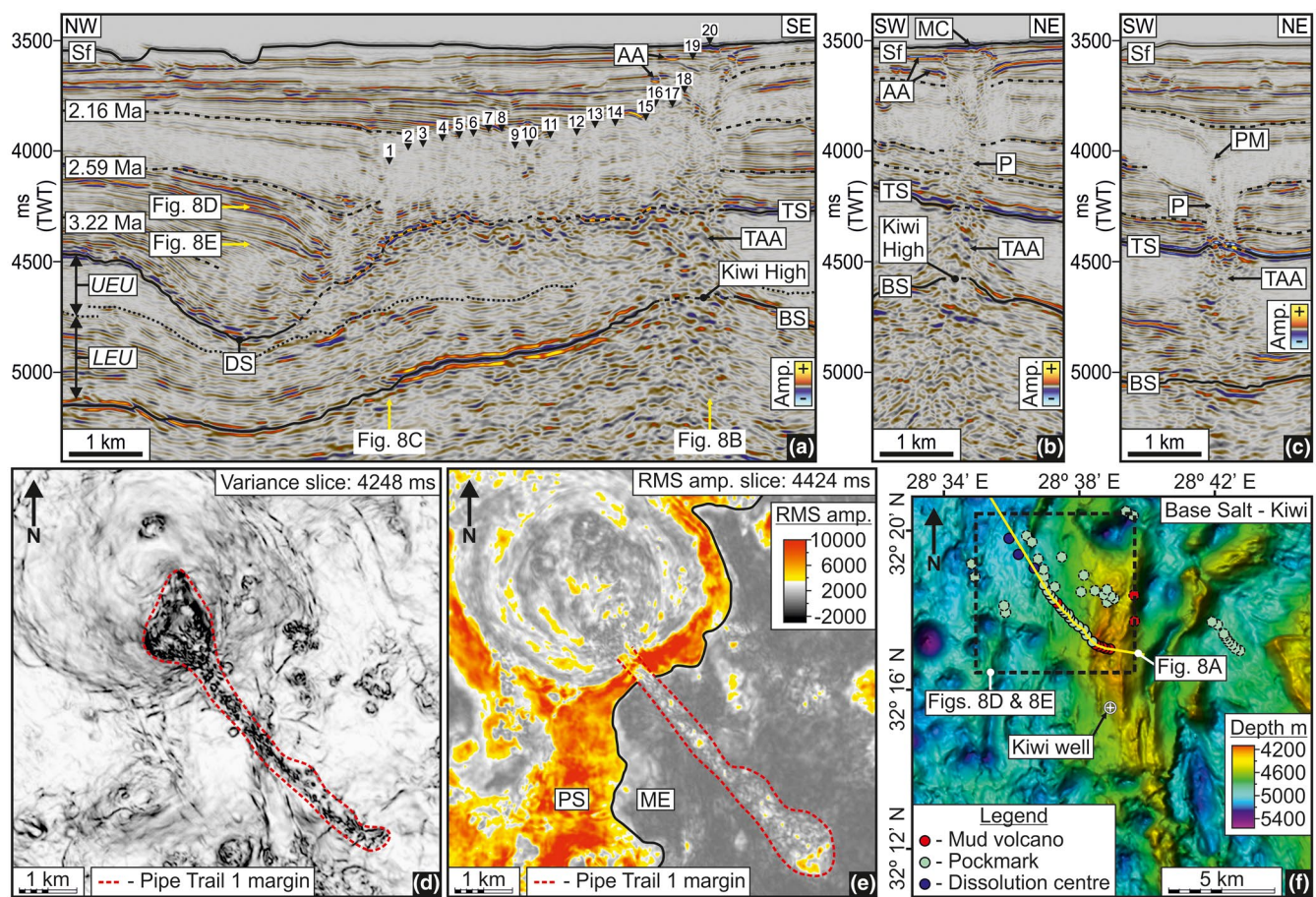


FIGURE 8 Pipe Trail 1 (the Kiwi Pipe Trail) overlying the Kiwi High at the Base Salt. (a) A seismic cross section (see Figure 8f for line location) through Pipe Trail 1 showing 20 pockmark and mud cone outlets positioned at progressively deeper horizons to the NW. (b) The most recently formed outlet (outlet 20; see Figure 8a for location) displays a mud cone (MC) at the seafloor (Sf) and directly overlies a trail of amplitude anomalies (TAA) through the Messinian Evaporites that extend downward to the Kiwi High at the Base Salt. Acoustically soft amplitude anomalies (AA) are distributed around the outlet. (c) The oldest pipe (P) in Pipe Trail 1 (outlet 1; see Figure 8a for location) displays a pockmark (PM) at its upper surface at approximately 2.3 Ma (± 0.25 Myrs). BS—Base salt; TS—Top Salt; LEU—Lower Evaporitic Unit; UEU—Upper Evaporitic Unit; DS—Dissolution structure. (d) A variance slice through the Post Salt Unit (see Figure 8a for location) that highlights Pipe Trail 1's planform as a NW-SE oriented linear trail of discontinuity. (e) A RMS amplitude slice through part of the Messinian Evaporites (ME) and Post Salt Unit (PS; see Figure 8a for location). Pipe Trail 1 is highlighted in the Messinian Evaporites as a NW-SE oriented linear distribution of amplitude anomalies. (f) A map of the Base Salt (see Figure 4a for location) showing the Kiwi High and the distribution of pockmarks and mud volcanoes overlying it

of the outlets in all the linear trails increases toward the NW and the most south-easterly outlet in each trail can be seen at the present day seafloor, implying recent activity (Figures 7 and 8). The outlets consist of both pockmarks and pockmarks overlain by small mud cones (volcanoes). The five pipe trails are described in detail in the following sections, with characteristics and dimensions summarised in Table 1. The majority of the description focuses on Pipe Trail 1 as a representative example, followed by details that are specific to the other four pipe trails.

The pipes in all of the linear trails are interpreted to transect the Messinian Evaporites and root to the Base Salt (cf. Cartwright et al., 2018). It seems most likely that the OM2 Unit has provided a sufficient flow of fluids for protracted fluid expulsion and intermittently mud in the ascending flow to form both pockmark and mud volcano outlets. In keeping with previous interpretations of pipes transecting thick salt layers in this area and elsewhere, we consider that they must have formed by hydraulic fracturing (Cartwright et al., 2021; Kirkham et al., 2018b).

4.3.1 | Pipe Trail 1

Pipe Trail 1 is located in the north-eastern part of the study area (Figure 4a). Its locus is represented by a mud cone at the present day seafloor with modest relief of ca. 10 m that is the outlet for an underlying pipe (Figure 8a–c). Twenty pipe-outlet combinations were identified at progressively deeper horizons in a north-westerly direction using the variance attribute cube in combination with seismic profiles (Figure 8a–d). Six of these outlets for the pipes in the trail are small mud cones with the remainder being pockmarks (14; Table 1). The pipes are spaced ca. 139–416 m (234 m average) apart and there is no systematic distribution of outlet types (pockmarks versus mud cones). The oldest outlet in the linear trail (Figure 8a,c) formed at ca. 2.3 Ma (± 0.25 Myrs) and is 4,255 m from the position of the youngest outlet, a mud cone that erupted within the Holocene (Figure 8a). ‘Soft’ localised amplitude anomalies are distributed adjacent to the mud volcanoes and pockmarks (Figure 8a,b), and are interpreted as evidence for the involvement of gas migration during pipe formation (cf. Kirkham et al., 2019; Oppo et al., 2020), further strengthening the interpretation that the pipes root beneath the salt.

The pipes are not clearly imaged within the Messinian Evaporites, unlike those reported from the Levant Basin (Cartwright et al., 2018; Kirkham et al., 2019; Oppo et al., 2020). However, irregularly dipping clustering of amplitude anomalies within the salt may be indicative of their generalised position within the salt (Figure 8a–c,e).

TABLE 1 Details and statistics from Pipe Trails 1–5

Pipe Trail	Number of pipes	Number of pockmarks	Number of mud volcanoes	Pipe seismic width range (m)	Pipe spacing range (m)	Average pipe spacing (m)	Age of first pipe and outlet (Ma; ± 0.25 Myrs)	Pipe trail length (m)	Average pipe trail strike	Average flow velocity (mm/yr ± 0.3 mm/yr)
1	20	14	6	76–291	139–416	234	2.3	4,260	321° NW	1.9
2	15	10	5	74–402	149–578	317	2.2	3,830	320° NW	1.7
3	27	21	6	53–185	120–602	251	3.3	6,330	321° NW	1.9
4	23	12	11	51–224	138–944	260	2.2	5,610	324° NW	2.6
5	13	6	7	119–367	146–813	383	2.2	4,270	322° NW	1.9

The youngest pipe in the trail transects 770 m of the Post Salt Unit and 820 m of Messinian Evaporites within which a vertical stack of amplitude anomalies can be observed (Figure 8b). In contrast, the oldest pipe transects only 480 m of Pliocene stratigraphy and amplitude anomalies are present only within the upper part of the Upper Evaporitic Unit (Figure 8c). RMS attribute analysis shows that the linear trail of pipe outlets corresponds directly to an underlying linear distribution of amplitude anomalies within the Upper Evaporitic Unit (Figure 8e). The youngest pipe emanates from the shallowest crestal position mapped at the Base Salt (Figure 8a,b) of an erosional remnant high named Kiwi (location of the Kiwi well; Figures 4 and 8f). In contrast, there is no obvious structural high at the Base Salt directly underlying the oldest pipe in the linear trail.

The Messinian Evaporites thin from 1,600 to 755 m above the crest of the Kiwi High and the smooth and regular geometry of the Top Salt is divergent to the relief at the Base Salt (Figure 8a,b). The Lower Evaporitic Unit thins onto the Kiwi High from up to 480 m to ca. 80 m directly above the Base Salt crest (Figure 8a).

4.3.2 | Pipe Trail 2

Pipe Trail 2 is located in the northern part of the 3D seismic survey (Figure 4a). The outlets for the 15 pipes in the linear trail are predominantly small mud cones (Figures 4a and 7a; Table 1). The age of the oldest pockmark is ca. 2.2 Ma (± 0.25 Myrs) and the most recent mud cone is located at the seafloor directly above the crest of a Base Salt high (Figure 7a).

4.3.3 | Pipe Trail 3

Pipe Trail 3 is the longest of the linear trails (6,330 m) and is also composed of the greatest number of pipes (27), the majority of which have pockmarks at their outlets (Figure 7b; Table 1). The linear trail is located in the central region of the 3D seismic survey (Figure 4a). The oldest outlet is a pockmark dated at ca. 3.3 Ma (± 0.25 Myrs; Figure 7b). Uniquely, the most recent outlet is a large mud volcano that has formed a large depletion 'bowl' at the Base Salt (Figure 7b).

4.3.4 | Pipe Trail 4

Pipe Trail 4 is ca. 8 km northeast of the Menes Caldera depression (Dupré et al., 2014; Huguenot et al., 2009; Figure 4a) and contains almost even numbers of pockmarks (12) and mud cones (11) at the outlets (Figures 4a and 7c). The Base Salt underlying the linear trail is mostly smooth, with a

discrete crestal high geometry directly underlying the most recent pipes (Figure 7c). The most north-westerly outlet in Pipe Trail 4 is dated as ca. 2.2 Ma (± 0.25 Myrs).

4.3.5 | Pipe Trail 5

Pipe Trail 5 is located only ca. 2 km west of Pipe Trail 4 (Figure 4a) and contains the fewest pipes (13) of all the linear trails (Figures 4a and 7d). The most north-westerly outlet in this linear trail is the same age (ca. 2.2 Ma ± 0.25 Myrs) as the most basinward in Pipe Trail 4. The Base Salt structure here is that of an elliptically shaped high directly underlying the linear trail (Figure 7d).

4.3.6 | Kinematic interpretation of the pipe trails

The linear trails described here are analogous in many respects to the linear fluid escape pipe trails described by Cartwright et al. (2018) and Kirkham et al. (2019) offshore Lebanon that record salt flow through episodic expulsion. Pipe Trails 1–5 all exhibit alternation in the outlet type, with sporadic occurrence of small mud cones interspersed with pockmark craters, similar in many respects to the pipe trails described by Oppo et al. (2020) offshore Lebanon. Each expulsion episode forms a new pipe through the Messinian Evaporites and an outlet at a contemporaneous seafloor. For Pipe Trails 1–5, we infer that the outlet was systematically offset to the NW through time due to basinward translation of the Post Salt Unit during salt flow, explaining the progressively older ages of outlets to the NW in all five trails.

The distance that the oldest outlet in each of the linear trails has been offset from its original location overlying a pre-salt fluid locus records the translation distance. We assume here, that the locus of pre-salt fluid expulsion remains static in its basinal context, whereas the overburden is translated by salt flow. All five trails emanate from erosional remnant highs as mapped at the Base Salt, so we consider this a reasonable assumption.

The age span from the oldest to youngest outlets records the interval of time over which this translation has taken place, from which the translation velocity is calculated (Table 1). For example the oldest outlet in Pipe Trail 1 is dated as ca. 2.3 Ma (± 0.25 Myrs) and the youngest is effectively the present day, and they are 4,360 m apart. Hence the average translation velocity during the period of fluid escape is ca. 1.9 mm/yr (± 0.3 mm/yr; see Table 1). The salt may have been flowing earlier, but we can only constrain the flow during the period in which episodic fluid expulsion occurred.

By comparison, the other four pipe trails record translation distances of 3,830–6,330 m, and comparable average

translation velocities of ca. 1.7–2.6 mm/yr (± 0.3 mm/yr; Table 1). Since the pipes intersect the Top Salt vertically, the translation distance recorded from the gross trail length and the respective average velocity values corresponding to these are equal to those at the top of the Messinian Evaporites. There is no evidence in any form of seismically visible detachment to suggest that the overburden is decoupled from the Top Salt. Hence the translation velocities obtained from the pipe trails are interpreted to represent the flow velocity in the uppermost part of the salt sequence, consistent with the conclusions as to overburden-salt coupling in Cartwright et al. (2018) and Oppo et al. (2020).

4.4 | Dissolution structures

Located a few kilometres northwest of the Base Salt erosional remnant the Kiwi High are two bowl-shaped

(concave-upward) depressions at the Top Salt (Figure 9a). Both depressions have a strikingly circular planform with diameters of 2,980 and 4,100 m, and relief of 370 and 530 m respectively. Within the depressions, the stratal geometries within part of the Pliocene interval are indicative of progressive development of the bowl-shaped subsidence of each depression (Figure 9b), with incremental growth packages that onlap within the depression (Figure 9c). In contrast to the numerous depressions at the Top Salt in the study area that have formed due to collapse above a mud volcanoes depletion zone in the Pre Salt Unit (Figure 5a; Kirkham et al., 2017), these top salt depressions are not infilled by mud volcanoes. Concentric normal faults with minor throws of <40 m are arranged around the periphery of the two depressions (Figure 9d).

The Messinian Evaporites thin systematically beneath the top salt depressions such that the loss of salt is matched by the volume of the infilling stratigraphy (Figure 9b). The

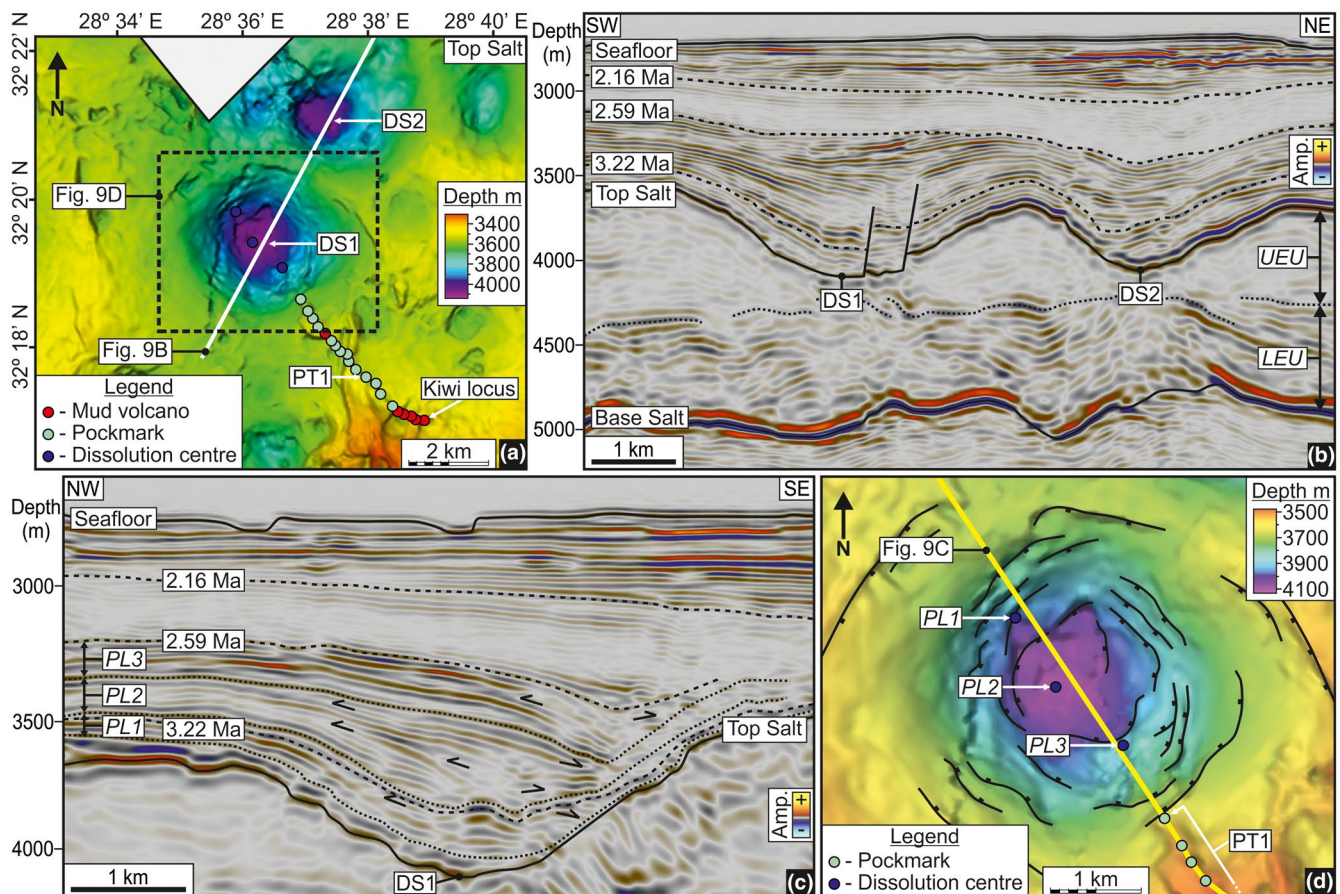


FIGURE 9 Dissolution structures basinward of Pipe Trail 1. (a) A map of the Top Salt showing two bowl-shaped depressions labelled DS1 and DS2 (DS = Dissolution structure) and the location of the mud volcanoes and pockmarks that comprise Pipe Trail 1 (PT1). (b) A seismic cross section (see Figure 9a for line location) through DS1 and DS2 showing depressions at the Top Salt and thinning of the Upper Evaporitic Unit (UEU) but no thinning of the Lower Evaporitic Unit (LEU). (c) A seismic cross section through DS1 along strike of Pipe Trail 1 (see Figure 9d for line location). The Pliocene Subunits PL1–PL3 thicken into the depression, with divergent reflections that concentrically onlap the internal margins of DS1. (d) A zoomed map of the Top Salt at DS1 (see Figure 9a for line location) showing concentric normal faults, the thickest points (centres) of PL1–PL3 and the most basinward pipes in Pipe Trail 1

circular planform, progressive infill geometry, peripheral fault system and the volumetric deficit in the underlying salt are diagnostic of salt dissolution structures formed in response to subjacent dissolution of an evaporite sequence by focused flow of undersaturated basin fluids (Bertoni & Cartwright, 2005). As such, we interpret the two depressions as having been formed by focused flow of pore water dissolving salt from focal points within the Pre Salt Unit. The two dissolution structures interpreted here are named Dissolution Structure 1 and Dissolution Structure 2 (DS1 and DS2, Figure 9a,b).

The Pliocene succession within DS1 is subdivided into three seismic-stratigraphic units (PL1–PL3; Figure 9c). The timing of growth of the depression was interpreted from the concentric onlap geometries and thickness relationships of the stratigraphy within the depressions (Figure 9c; cf. Bertoni & Cartwright, 2005). The onset of the dissolution phase is interpreted as ca. 4.3 Ma (± 0.5 Myrs) for both DS1 and DS2 and the termination of dissolution is ca. 2.6 and 2.9 Ma (± 0.25 Myrs) respectively.

An interesting feature of detailed isopach mapping of the fills for DS1 and DS2 is that there is a systematic lateral shift in the maximum thickness position of each growth package within the depressions. This is seen very clearly in DS1, with a progressive younging to the SE (Figure 9c,d). These isopach maximum loci are distributed directly along strike to the NW of Pipe Trail 1 (Figure 9d), with the centre of PL1 located 900 m from the oldest pipe in Pipe Trail 1 and 5,130 m from the youngest pipe overlying the Kiwi High at the Base Salt. DS2 is located 5,300 m northwest from the crestal area of the Kiwi High.

The accommodation space created within the depressions of DS1 and 2 are ca. 2.5 and 1.25 km³, respectively, and represents the volume of Messinian Evaporites that have been dissolved locally during their formation (cf. Bertoni & Cartwright, 2005). The loss of salt volume is restricted to the Upper Evaporitic Unit (Figure 9b), and results in grounding of the Top Salt against the interface between Upper and Lower Evaporitic Units. The Base Salt underlying DS1 and DS2 is relatively flat lying and discordant to the depression at the Top Salt, with no pre-salt structures directly underlying the dissolution structures (Figure 9b).

We interpret that the backstepping depocentres for PL1–PL3 are the result of basinward salt flow and translation of the Post Salt Unit to the northwest contemporaneous with dissolution above a static pre-salt fluid locus. The distribution of the PL1–PL3 depocentres in DS1 directly along the strike of Pipe Trail 1 indicates that the source of focused fluids for dissolution was most probably the Kiwi High. Dissolution was concentrated within the Upper Evaporitic Unit due to the crestal region of the Kiwi High

being almost exclusively overlain by the Upper Evaporitic Unit (see Section 4.3.1). Conservatively, salt flow in this part of the basin must have commenced some time within Subunit PL1 to account for the local isopach maximum, or at the very latest just prior to deposition of Subunit PL2. We tentatively suggest an onset age for the dissolution at ca. 4.3 Ma (± 0.5 Myrs) based on the uncertainty in defining the initial onlap fill. DS1 and DS2 record 5,130–5,300 m of translation respectively. If we conservatively take the onset to salt flow as the boundary between Subunits PL1 and PL2 at ca. 3.2 Ma (± 0.25 Myrs), this yields an average flow velocity for these kinematic markers of ca. 1.6 mm/yr (± 0.3 mm/yr). Since the average velocity computed for the Kiwi Pipe Trail (PT1) is 1.9 mm/yr (± 0.3 mm/yr), it is conceivable that the initial phase of salt flow expressed in the lateral migrating fill of PL1–3 was much slower than the later phase expressed in the pipe trail, but this inference is subject to the uncertainties of using average sedimentation rates as a dating method.

4.5 | Lateral displacement of mud volcanoes from their depletion zones

Detailed mapping of mud volcanoes and their corresponding depletion zones was undertaken in a sub-area (A) located within the southern section of the study area (Figures 4a and 10a). Area A was selected for detailed mapping because: (1) it contains only five mud volcanoes (MV1–MV5; Table 2) that are all Early Pliocene in age; (2) the depletion zones (DZ1–DZ5) for these Early Pliocene mud volcanoes have not been overprinted by several younger phases of mud volcanism, in contrast to the central mud volcano field (see Section 4.1.1).

MV1–MV5 have significant areas and volumes (see Table 2), yet there is no clear depletion zone directly beneath any of these mud volcanoes. However, five depressions at the Base Salt (DZ1–DZ5) that have the seismic character of depletion zones (see Section 4.1.1) are located SSE of the mud volcanoes (Figure 10b,c; see Table 2 for statistics of DZ1–DZ5). Most significantly, the volumes within the depletion zones and mud volcanoes are approximately equal (e.g. DZ1 = 0.23 km³ and MV1 = 0.25 km³; Table 2). Approximate volume balancing of depletion zones and mud volcanoes has been demonstrated by Graue (2000), Kirkham et al. (2017) and Dupuis et al. (2019). The volumes of all five of the mud volcanoes and depressions at the Base Salt, as shown in Table 2, balance to within a maximum of 8% of each other, which strongly suggests that DZ1–DZ5 represent the depletion zones for MV1–MV5 (Figure 10a).

We interpret that the Early Pliocene aged mud volcanoes (MV1–MV5) in Area A have been offset to the NNW

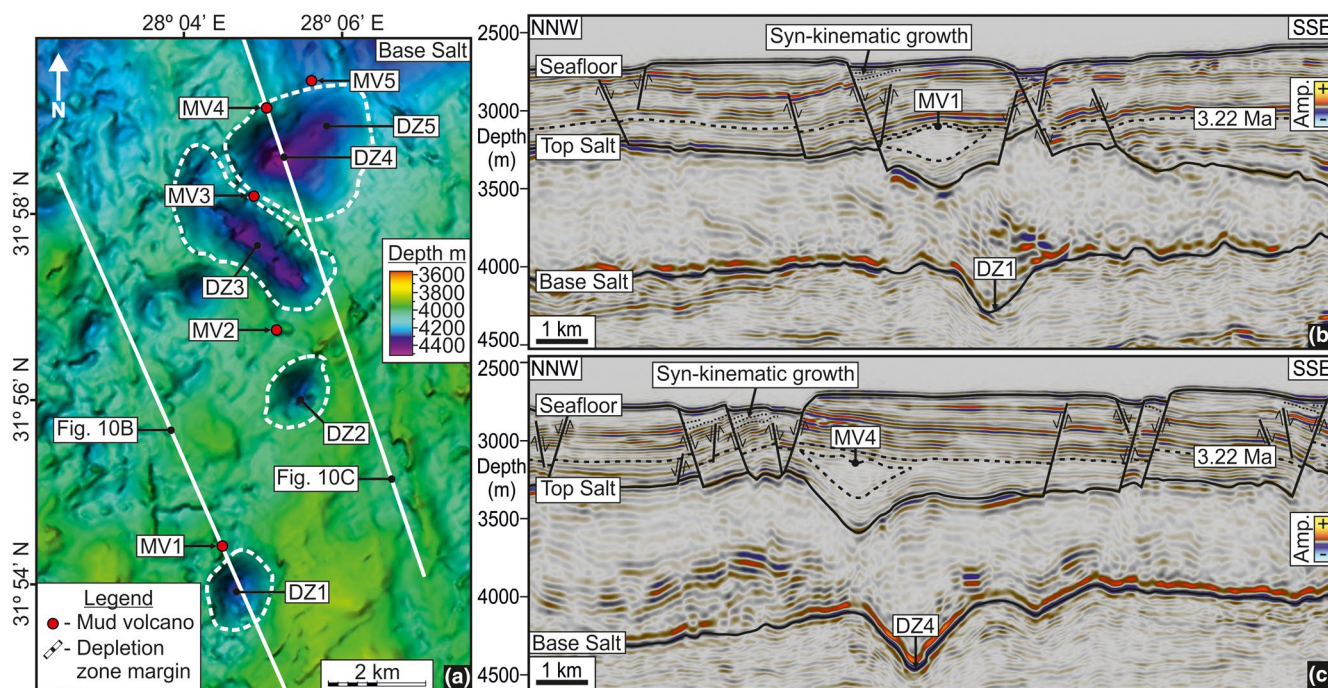


FIGURE 10 Mud volcanoes offset from above their depletion zones in Area A (see Figure 4a for location). (a) A map of the Base Salt in Area A showing five circular-irregularly shaped depletion zones (DZ1–DZ5) and the location of five mud volcanoes (MV1–MV5) that are all offset NNW of the depletion zones. (b and c) Seismic cross sections (see Figure 10a for line locations) through MV1 and DZ1, and MV4 and DZ4, showing that the Early Pliocene mud volcanoes that were originally aligned vertically with their depletion zones in the Pre Salt Unit have been offset to the NNW. The Post Salt Unit contains growth faults that detach in the Messinian Evaporites and record minor syn-kinematic growth since the Late Pleistocene

TABLE 2 Statistics from the offset depletion zones (DZ) and mud volcanoes (MV) in Area A highlighted in Figure 10 (location shown in Figure 4a). Statistics of MV4–MV5, and DZ4–DZ5 are given cumulatively because they closely overlap (Figure 10a) forming a composite edifice and composite depletion zone

Depletion zones (DZ)	Area (km ²)	Max relief (m)	Volume (km ³)	Mud volcanoes (MV)	Area (km ²)	Max thickness (m)	Volume (km ³)	DZ to MV distance (m)	Offset strike
DZ1	1.51	342	0.23	MV1	4.74	225	0.25	900	341 NNW
DZ2	1.33	309	0.13	MV2	2.46	173	0.12	1,400	339 NNW
DZ3	4.92	390	0.69	MV3	9.5	290	0.7	1,340	344 NNW
DZ4 & DZ5	5.82	444	0.63	MV4 & MV5	6.6	280	0.59	1,090	349 NNW

from their original position directly above the pre-salt depletion zones (DZ1–DZ5), by translation of the Post Salt Unit above the basinward flowing Messinian Evaporites, analogous to the pipe trails and dissolution structures. The translation distance from the centre of the mud volcanoes to the centre of the depletion zones range from 900 to 1,400 m (Table 2).

Over a hundred mud volcanoes distributed throughout the study area (Figure 4a) present further potential kinematic markers, although tracking their offsets from their respective depletion zones has not been undertaken in detail with the exception of three further examples of volcano-depletion zone pairs (Figure 11). In general,

however, we observe that the majority of the recently extruded mud volcanoes can be linked vertically to their depletion zone with little to no offset (Kirkham et al., 2017), whereas older mud volcanoes and their depletion zones no longer align vertically. It is clear that across the broader study area, the mud volcano plumbing systems can be used to acquire kinematic data in parts of the study area where there are no pipe trails or dissolution structures (Figures 11 and 12), filling in gaps in the observed patterns of regional salt flow. The flow direction and the magnitude of translation (6,400–7,500) recorded from other Early Pliocene mud volcano plumbing systems in the central and eastern sections of the study area are comparable to

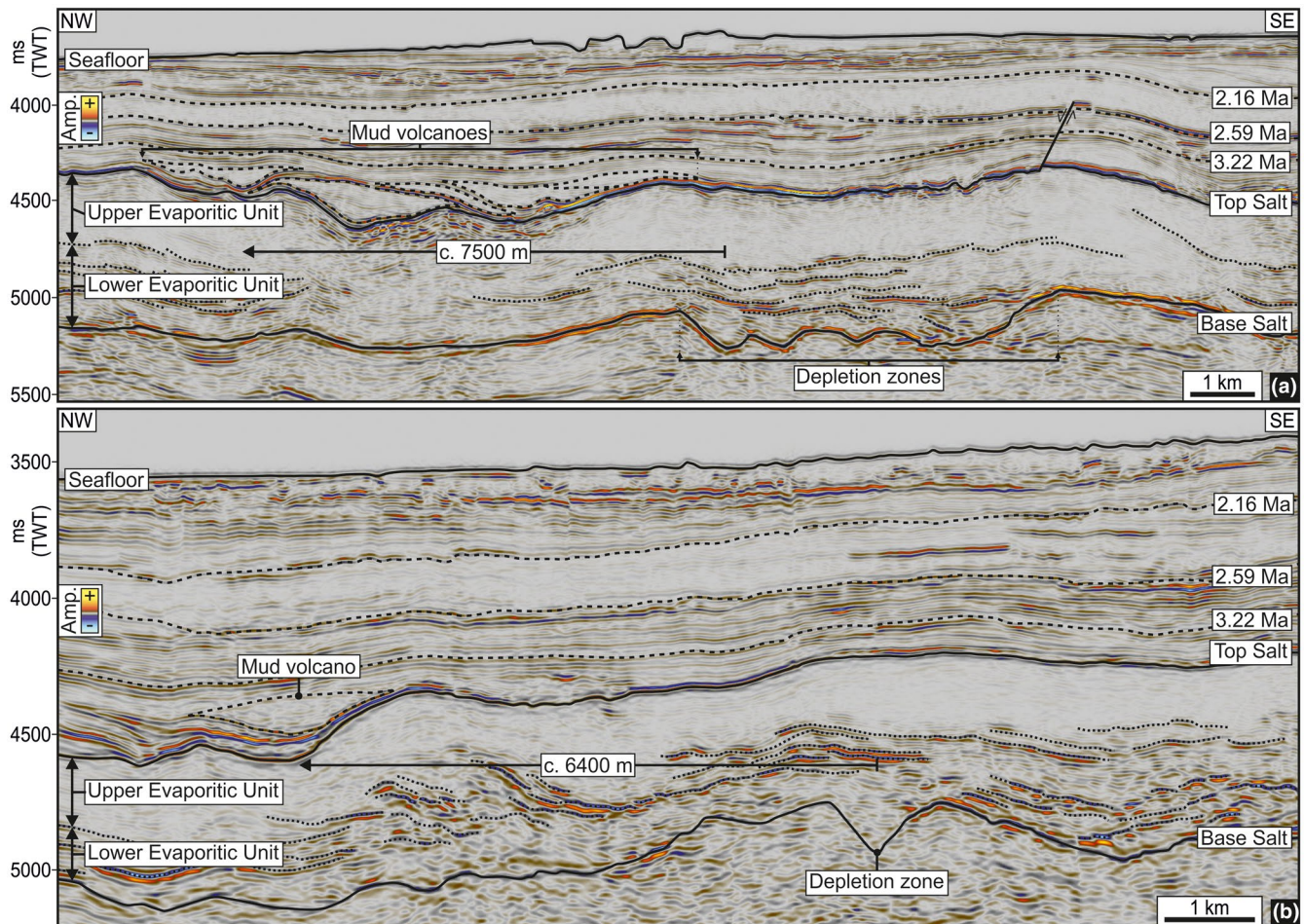


FIGURE 11 Mud volcanoes in the Post Salt Unit offset from their depletion zones in the Pre Salt Unit (see Figure 4a for line locations). (a) A seismic cross section showing several Early Pliocene mud volcanoes that have been translated ca. 7,500 m to the NW away from the original position vertically overlying a composite depletion zone in the Pre Salt Unit. (b) A single Early Pliocene mud volcano that has been offset ca. 6,400 m from its depletion zone in the Pre Salt Unit

those recorded from the pipe trails and dissolution structures (Figures 11 and 12).

5 | DISCUSSION

5.1 | Kinematic markers for salt flow

The preceding sections demonstrate that displaced mud volcanoes, mud volcano conduits and displaced dissolution structures can add to previously documented geological features such as salt-detached ramp syncline basins (Jackson & Hudec, 2005; Pichel et al., 2018), deformed fluid escape pipes (Cartwright et al., 2018; Kirkham et al., 2019) and deformed intra-salt structures (Kirkham & Cartwright, 2021) as a growing suite of potential kinematic markers for reconstructing salt flow (Figure 12).

The identification of these new types of kinematic markers opens a promising avenue for further research in this area of salt tectonics. A suite of kinematic markers within

a defined area that has been subject to gravity-driven deformation of salt, for example allows direct comparisons to be made with the inferred flow patterns derived from overburden deformation such as growth faults in the extensional domain or detachment folds in the contractional domain (cf. Anderson et al., 2000; Letouzey et al., 1995; Peel, 2014; Rowan et al., 2004; Worrall & Snelson, 1989). To illustrate the potential utility of these novel kinematic markers, we attempt to place our observations into a wider context of the salt tectonic deformational history of this segment of the basin margin (Figure 12).

5.2 | Kinematics of the West Nile Delta Province

5.2.1 | Flow direction and timing

The kinematic data derived from the kinematic markers in the study area are shown in Figure 12. The almost

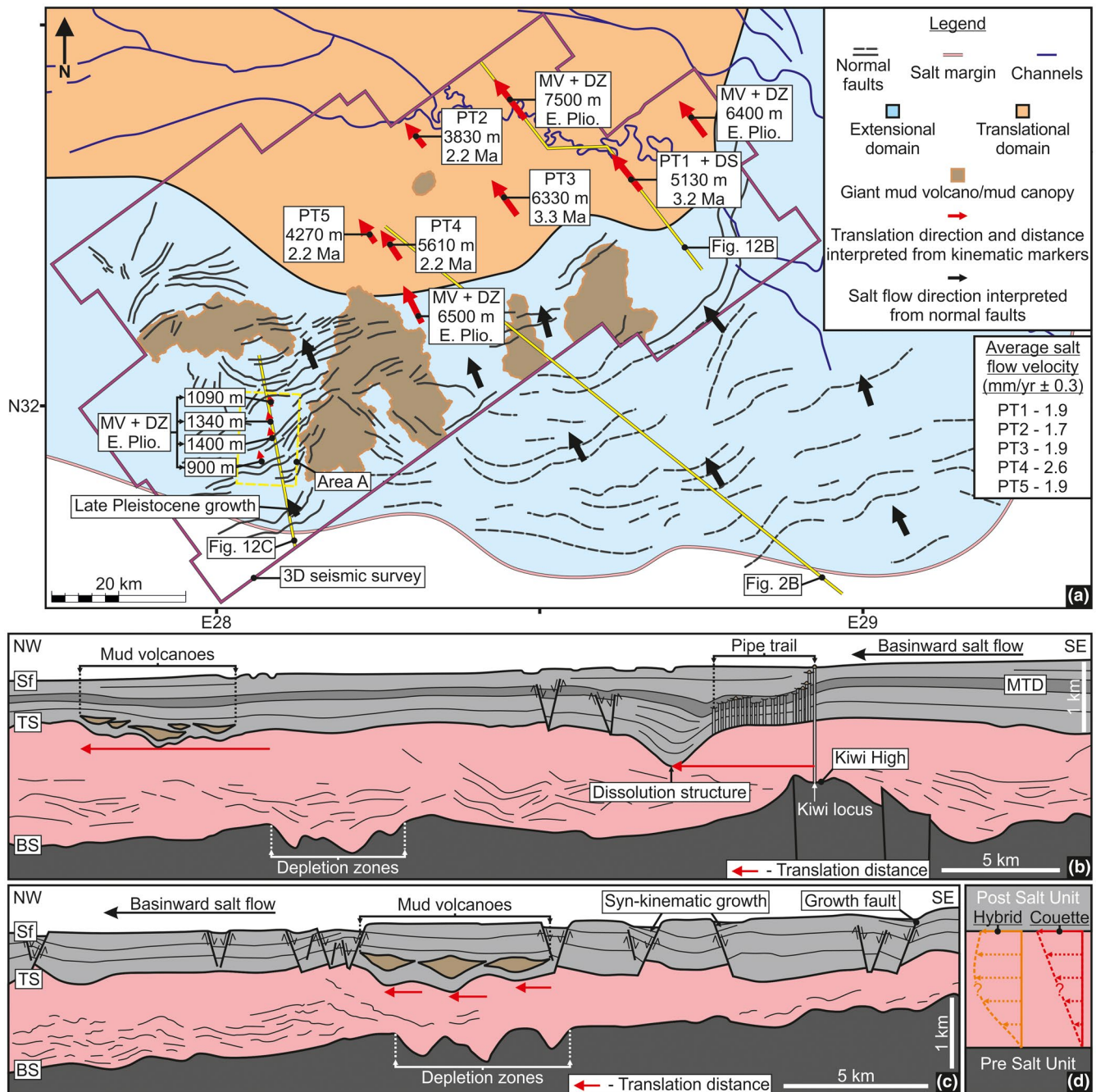


FIGURE 12 Naturally forming kinematic markers for salt flow in the western Nile. (a) A map of the study area showing the salt margin (modified from Lofi et al., 2011; Loncke et al., 2006), the extensional and translational domains of the salt basin, the distribution of seafloor channels and normal faults (modified from Loncke et al., 2006—dashed black lines; new interpretation—solid black lines), and the location of the giant mud volcanoes/mud canopies (Kirkham et al., 2018a) on top of the Messinian Evaporites. The black arrows represent the salt flow direction interpreted from growth fault orientations. The red arrows represent salt flow directions recorded from the kinematic markers described in this study. The length of the red arrows is equal to the amount of translation recorded from each kinematic marker. Annotation for the type of kinematic marker, amount of translation and timing (± 0.25 Myrs) from when the kinematic marker records salt flow are given. PT—Pipe trail; DS—Dissolution structure; MV—Mud volcano; DZ—Depletion zone; E. Plio.—Early Pliocene. (b) A cross section that demonstrates the basinward translation of a pipe trail and dissolution structure away from a pre-salt fluid locus (the Kiwi High), as well as mud volcanoes in the Post Salt Unit that are offset from their depletion zones in the Pre Salt Unit. (c) A cross section from the southwest of the study area showing the translation of three Early Pliocene mud volcanoes basinward of their depletion zones in the Pre Salt Unit as a result of salt flow, as well as growth faults that detach in the Messinian Evaporites and formed in the Late Pleistocene-Holocene. Sf—Seafloor; MTD—Mass transport deposit; TS—Top salt; BS—Base salt. (d) A schematic of the possible flow regimes through the salt in the study area. A Couette flow regime is the simplest explanation for the observations from the kinematic markers, however, a more complex hybrid between Couette and Poiseuille cannot be ruled out

uniform NW orientation of the kinematic markers is consistent with the Pliocene-Recent basinward flow direction implied from the normal fault orientation in the extensional domain and the strike of detachment folds and thrusts in the contractional domain (Figure 12). Caution needs to be applied to this latter point, because of the likely involvement of basement involved thrusts associated with the Mediterranean Ridge displacing salt to the SE (Allen et al., 2016).

The kinematic markers not only demonstrate unidirectional flow in the translation domain (320° – 324°) over a fairly extensive area (ca. 3,000 km²; Figure 12), but also show that this flow was consistent over a prolonged period of ca. 3 Myrs. The only deviation from this general NW flow direction is recorded by the track of the offset mud volcanoes in Area A to a NNW flow direction (Figure 12). This is interpreted as due to a change in strike of the landward limit of the Messinian Evaporites to the south of Area A (Figure 12). It is also possible that the location of the giant mud volcanoes/mud canopies (see Section 4.2.1; Figures 4a and 12) with their elongate feeders through the salt (Kirkham, Cartwright, et al., 2020; Kirkham et al., 2018a) could have contributed in channelling the flowing salt, resulting in minor modification in the flow direction.

The question of the timing of salt flow is much more problematic. The pipe trails provide the clearest evidence of the longevity of salt flow in a specific direction but they do not by themselves record the onset of salt flow. They only capture the time window over which episodic fluid venting occurred. In the case of the dissolution structures associated with the Kiwi High (Figure 9), the time span of salt flow could be extended backwards in time by genetically linking the fluid expulsion necessary for dissolution with that required for pipe and outlet formation in Pipe Trail 1. This pushed the period of known salt flow back to at least the Late Pliocene (3.2 Ma), and possibly as far back as the Early Pliocene (ca. 4 Ma). The displaced mud volcanoes are in essence singular fluid expulsion events, and as such provide no calibration of the period of salt flow. All that can be inferred is that the translation occurred at some time after the mud volcano was erupted. From all the available kinematic data, we can therefore only provide loose constraints on the onset of salt flow in the area being from the Early Pliocene, most likely some time between 4 and 3.2 Ma. This onset of salt flow is however consistent with interpretation of growth packages of Early Pliocene age on the salt-detached normal faults in the extensional domain (Figure 2b). The onset of growth on faults in the southwest of our study area is, in contrast, Late Pleistocene in age (Figures 6b and 10b,c), suggesting that there may be some diachroneity in the initiation of gravity-driven deformation and salt flow along the strike

of the basin margin. A Late Pleistocene onset to salt flow in Area A may well explain the lesser translation distances recorded from the mud volcanoes offset from their depletion zones in Area A (Figures 10 and 12a,c; Table 2). Similar diachroneity is well documented along the margin of the Levant Basin (Cartwright & Jackson, 2008; Elfassi et al., 2019).

5.2.2 | Salt flow velocity

In addition to the remarkable constancy of flow direction in the study area, the average flow velocities computed from the kinematic markers also exhibit a very narrow range of values (Table 1). The pipe trails provide the best data because of the most accurate age control. The older mud volcanoes in particular, and the early history of the dissolution structures are quite loosely dated, and hence the average velocity values carry greater uncertainty. Nevertheless, all the measurements fall in the range 2 mm/yr (± 0.6 mm/yr). These values are comparable to the spread in average velocities measured from pipe trails in the Levant Basin (Kirkham et al., 2019; Oppo et al., 2020) and where the velocity was used to estimate bulk viscosity of the salt (Cartwright et al., 2018).

The consistency in salt flow direction and velocity over such a large area can only be recorded because of the good spread of kinematic markers over the study area and is intriguing considering the changes in salt thickness and considerable Base Salt topography. This prompts a number of questions such as why does the relief at the Base Salt have so little influence on the flow characteristics? This emphasises the value to salt tectonics of finding such markers for salt flow kinematics.

Unfortunately, and unlike the previous studies from offshore Lebanon, the kinematic markers in our study area have not provided direct constraints on the internal (vertical) velocity variation within the salt sequence. Offshore Lebanon, the 3D seismic processing was able to image the deformed pipes (Cartwright et al., 2018; Oppo et al., 2020), but in the survey used for this study, neither the offset mud volcano conduits or deformed pipes have been imaged, and instead, cryptic traces of stacked amplitude anomalies are the only signs that fluid transfer has occurred through the salt (Figures 7 and 8).

What then, can be inferred for the likely internal flow regime? We tentatively suggest that the consistency in the flow direction and translation distances is most compatible with a fairly simple flow regime, and that this is likely to be close to an idealised Couette flow. Numerical and analogue models of flow in the translation domain of a gravity tectonic system driven by simple tilting show

that classical Couette profile is to be expected within thick salt layers at depth (Albertz & Ings, 2012; Brun & Merle, 1985; Gemmer et al., 2004; Peel, 2014; Quirk et al., 2012; Schultz-Ela, 2001). We can rule out a simple Poiseuille flow regime, because this would not result in the translations observed. Poiseuille flow is generally predicted where there is a significant component of differential loading (Albertz & Ings, 2012; Gemmer et al., 2004; Ings et al., 2004; Peel, 2014; Rowan et al., 2004), but as Zucker et al. (2020) have recently argued, that is not the case here in the western province of the Nile Delta and Nile Deep Sea Fan. These latter authors have proposed tilting of the basin as the principal driver in this western province, which is endorsed by our interpretation of the kinematic data. In summary, Couette flow seems to be the simplest interpretation of the flow regime during the Pliocene to Recent here (Figure 12d), but we cannot exclude more complex flow profiles hybrid between Couette and Poiseuille (Figure 12d), especially since there may be subtle influence of intra-salt heterogeneity on the flow regime that are not currently calibrated.

Although in this study area there remains some uncertainty over the precise nature of the flow regime and the onset of salt flow, the added value of knowing the precise translation distances travelled by the coupled overburden and top salt are an invaluable addition to the analytical armoury to tackle salt tectonic problems. It seems likely that more kinematic markers will be added to the growing catalogue of these invaluable features, particularly with the expanding access to high-resolution 3D seismic surveys in salt basins worldwide. These will surely be as invaluable in other salt basins as they have proved to be in the Eastern Mediterranean.

6 | CONCLUSIONS

The major conclusions of this study are as follows:

1. Mud volcano conduits, mud volcano edifices displaced from their depletion zones and displaced dissolution structures can be added to the growing list of naturally forming geological phenomena that can be used as kinematic markers to constrain the salt flow direction, overburden translation distance and flow velocity at the top of a salt layer.
2. Salt flow in the western Nile province is unidirectional to the NW throughout the Pliocene–Recent, and is approximately perpendicular to the continental margin and pinch-out of the Messinian Evaporites.
3. The average salt flow velocity is of the order of 2 mm/yr (± 0.6 mm/yr) over an area of ca. 3,000 km² of the outer extensional domain/inner translational domain.
4. The kinematic markers and salt-detached growth faults in the extensional domain suggest there may be a diachronous onset to salt flow along strike of the basin margin.
5. Multi-kilometre translation distances, coupling of the top of the Messinian Evaporites and base of the Post Salt, and a gravity gliding driver for salt tectonic deformation are most simply explained by a Couette flow regime.

ACKNOWLEDGEMENTS

We thank the editor Craig Magee and the reviewers Tiago Alves and Mike Hudec for their considered and constructive comments that led to an improved manuscript. Thank you to the seismic lab team in Oxford, particularly Claudia Bertoni, for the many helpful discussions. We are grateful to Equinor for provision of the 3D seismic data. We thank Schlumberger for provision of the seismic interpretation software.

CONFLICT OF INTEREST

There are no conflicts of interest to declare.

PEER REVIEW

The peer review history for this article is available at <https://publons.com/publon/10.1111/bre.12612>.

DATA AVAILABILITY STATEMENT

The data used for this research are confidential industry seismic reflection data and cannot be shared.

REFERENCES

- Albertz, M., & Ings, S. J. (2012). Some consequences of mechanical stratification in basin-scale numerical models of passive-margin salt tectonics. *Geological Society, London, Special Publications*, 363, 303–330. <https://doi.org/10.1144/SP363.14>
- Allen, H., Jackson, C.-A.-L., & Fraser, A. J. (2016). Gravity-driven deformation of a youthful saline giant: The interplay between gliding and spreading in the Messinian basins of the Eastern Mediterranean. *Petroleum Geoscience*, 22, 340–356. <https://doi.org/10.1144/petgeo2016-034>
- Anderson, J., Cartwright, J., Drysdall, S., & Vivian, N. (2000). Controls on turbidite sand deposition during gravity-driven extension of a passive margin: Examples from Miocene sediments in Block 4, Angola. *Marine and Petroleum Geology*, 17, 1165–1203. [https://doi.org/10.1016/S0264-8172\(00\)00059-3](https://doi.org/10.1016/S0264-8172(00)00059-3)
- Baer, S., Lie, Ø., & Almorshedy, A. (2016). New opportunities offshore West Egypt. *GEO ExPro Magazine*.
- Barber, P. M. (1981). Messinian subaerial erosion of the proto-Nile Delta. *Marine Geology*, 44(3–4), 253–272. [https://doi.org/10.1016/0025-3227\(81\)90053-0](https://doi.org/10.1016/0025-3227(81)90053-0)
- Bertoni, C., & Cartwright, J. (2005). 3D seismic analysis of circular evaporite dissolution structures, Eastern Mediterranean. *Journal of the Geological Society*, 162, 909–926. <https://doi.org/10.1144/0016-764904-126>

- Brown, A. R. (2004). Interpretation of three-dimensional seismic data. AAPG memoir 42, SEG investigations in geophysics 9. Society of Exploration Geophysicists and American Association of Petroleum Geologists. 31–60. <https://doi.org/10.1190/1.9781560802884.ch2>
- Brun, J.-P., & Fort, X. (2011). Salt tectonics at passive margins: Geology versus models. *Marine and Petroleum Geology*, 28, 1123–1145. <https://doi.org/10.1016/j.marpetgeo.2011.03.004>
- Brun, J. P., & Merle, O. (1985). Strain patterns in models of spreading-gliding Nappes. *Tectonics*, 4, 705–719. <https://doi.org/10.1029/TC004i007p00705>
- Cartwright, J. A., & Jackson, M. P. A. (2008). Initiation of gravitational collapse of an evaporite basin margin: The Messinian saline giant, Levant Basin, eastern Mediterranean. *Geological Society of America Bulletin*, 120, 399–413. <https://doi.org/10.1130/B26081X.1>
- Cartwright, J., Jackson, M., Dooley, T., & Higgins, S. (2012). Strain partitioning in gravity-driven shortening of a thick, multilayered evaporite sequence. *Geological Society, London, Special Publications*, 363, 449–470. <https://doi.org/10.1144/SP363.21>
- Cartwright, J., Kirkham, C., Bertoni, C., Hodgson, N., & Rodriguez, K. (2018). Direct calibration of salt sheet kinematics during gravity-driven deformation. *Geology*, 46, 623–626. <https://doi.org/10.1130/G40219.1>
- Cartwright, J., Kirkham, C., Foschi, M., Hodgson, N., Rodriguez, K., & James, D. (2021). Quantitative reconstruction of pore pressure history in sedimentary basins using fluid escape pipes. *Geology*, 49(5), 576–580. <https://doi.org/10.1130/G48406.1>
- Cartwright, J., & Santamarina, C. (2015). Seismic characteristics of fluid escape pipes in sedimentary basins: Implications for pipe genesis. *Marine and Petroleum Geology*, 65, 126–140. <https://doi.org/10.1016/j.marpetgeo.2015.03.023>
- Davison, I., Alsop, I., & Blundell, D. (1996). Salt tectonics: Some aspects of deformation mechanics. *Geological Society, London, Special Publications*, 100, 1–10. <https://doi.org/10.1144/GSL.SP.1996.100.01.01>
- Davison, I., Anderson, L., & Nuttall, P. (2012). Salt deposition, loading and gravity drainage in the Campos and Santos salt basins. *Geological Society, London, Special Publications*, 363, 159–174. <https://doi.org/10.1144/SP363.8>
- Dolson, J., Boucher, P., Siok, J., & Heppard, P. (2005). Key challenges to realizing full potential in an emerging giant gas province: Nile Delta/Mediterranean offshore, deep water, Egypt. *Geological Society, London, Petroleum Geology Conference Series*, 6, 607–624. <https://doi.org/10.1144/0060607>
- Dooley, T. P., Jackson, M. P., & Hudec, M. R. (2007). Initiation and growth of salt-based thrust belts on passive margins: Results from physical models. *Basin Research*, 19, 165–177. <https://doi.org/10.1111/j.1365-2117.2007.00317.x>
- Dupré, S., Mascle, J., Foucher, J.-P., Harmegnies, F., Woodside, J., & Pierre, C. (2014). Warm brine lakes in craters of active mud volcanoes, Menes caldera off NW Egypt: Evidence for deep-rooted thermogenic processes. *Geo-Marine Letters*, 34, 153–168. <https://doi.org/10.1007/s00367-014-0367-1>
- Dupuis, M., Imbert, P., Odonne, F., & Vendeville, B. (2019). Mud volcanism by repeated roof collapse: 3D architecture and evolution of a mud volcano cluster offshore Nigeria. *Marine and Petroleum Geology*, 110, 368–387. <https://doi.org/10.1016/j.marpetgeo.2019.07.033>
- Elfassi, Y., Gvirtzman, Z., Katz, O., & Aharonov, E. (2019). Chronology of post-Messinian faulting along the Levant continental margin and its implications for salt tectonics. *Marine and Petroleum Geology*, 109, 574–588.
- Feng, Y. E., Steinberg, J., & Reshef, M. (2017). Intra-salt deformation: Implications for the evolution of the Messinian evaporites in the Levant Basin, eastern Mediterranean. *Marine and Petroleum Geology*, 88, 251–267. <https://doi.org/10.1016/j.marpetgeo.2017.08.027>
- Flecker, R., Krijgsman, W., Capella, W., de Castro Martins, C., Dmitrieva, E., Mayser, J. P., Marzocchi, A., Modestou, S., Ochoa, D., Simon, D., Tulbure, M., van den Berg, B., van der Schee, M., de Lange, G., Ellam, R., Govers, R., Gutjahr, M., Hilgen, F., Kouwenhoven, T., ... Yousfi, M. Z. (2015). Evolution of the Late Miocene Mediterranean-Atlantic gateways and their impact on regional and global environmental change. *Earth-Science Reviews*, 150, 365–392. <https://doi.org/10.1016/j.earscirev.2015.08.007>
- Garcia-Castellanos, D., Estrada, F., Jiménez-Munt, I., Gorini, C., Fernández, M., Vergés, J., & de Vicente, R. (2009). Catastrophic flood of the Mediterranean after the Messinian salinity crisis. *Nature*, 462, 778–781. <https://doi.org/10.1038/nature08555>
- Garziglia, S., Migeon, S., Ducassou, E., Loncke, L., & Mascle, J. (2008). Mass-transport deposits on the Rosetta province (NW Nile deep-sea turbidite system, Egyptian margin): Characteristics, distribution, and potential causal processes. *Marine Geology*, 250, 180–198. <https://doi.org/10.1016/j.margeo.2008.01.016>
- Gemmer, L., Beaumont, C., & Ings, S. J. (2005). Dynamic modelling of passive margin salt tectonics: Effects of water loading, sediment properties and sedimentation patterns. *Basin Research*, 17, 383–402. <https://doi.org/10.1111/j.1365-2117.2005.00274.x>
- Gemmer, L., Ings, S. J., Medvedev, S., & Beaumont, C. (2004). Salt tectonics driven by differential sediment loading: Stability analysis and finite-element experiments. *Basin Research*, 16, 199–218. <https://doi.org/10.1111/j.1365-2117.2004.00229.x>
- Giresse, P., Loncke, L., Huguen, C., Muller, C., & Mascle, J. (2010). Nature and origin of sedimentary clasts associated with mud volcanoes in the Nile deep-sea fan. Relationships with fluid venting. *Sedimentary Geology*, 228, 229–245. <https://doi.org/10.1016/j.sedgeo.2010.04.014>
- Graue, K. (2000). Mud volcanoes in deepwater Nigeria. *Marine and Petroleum Geology*, 17, 959–974. [https://doi.org/10.1016/S0264-8172\(00\)00016-7](https://doi.org/10.1016/S0264-8172(00)00016-7)
- Gulmammadov, R. (2017). *Seismic geomechanics of mud volcanoes*. The University of Manchester.
- Hsü, K., Kj, H., Mb, C., & Wbf, R. (1973). The origin of the Mediterranean evaporites. *Initial Reports of the Deep Sea Drilling Project*, 13, 1203–1231.
- Huguen, C., Foucher, J. P., Mascle, J., Ondréas, H., Thouement, M., Gontharet, S., Stadnitskaia, A., Pierre, C., Bayon, G., Loncke, L., Boetius, A., Bouloubassi, I., de Lange, G., Caprais, J. C., Fouquet, Y., Woodside, J., & Dupré, S. (2009). Menes caldera, a highly active site of brine seepage in the Eastern Mediterranean sea: “In situ” observations from the NAUTINIL expedition (2003). *Marine Geology*, 261, 138–152. <https://doi.org/10.1016/j.margeo.2009.02.005>
- Ings, S., Beaumont, C., & Gemmer, L. (2004). Numerical modeling of salt tectonics on passive continental margins: Preliminary assessment of the effects of sediment loading, buoyancy, margin tilt, and isostasy. In *24th Annual GCSSEPM Foundation, Bob F.*

- Perkins Research Conference Proceedings (Vol. 36, p. 69). <https://doi.org/10.5724/gcs.04.24.0036>
- Jackson, M. P., & Hudec, M. R. (2005). Stratigraphic record of translation down ramps in a passive-margin salt detachment. *Journal of Structural Geology*, 27, 889–911. <https://doi.org/10.1016/j.jsg.2005.01.010>
- Jackson, M. P., & Hudec, M. R. (2017). *Salt tectonics: Principles and practice* (pp. 28–60). Cambridge University Press. <https://doi.org/10.1017/9781139003988>
- Kirkham, C. (2016). *A 3D seismic interpretation of mud volcanoes within the western slope of the Nile Cone*. Cardiff University.
- Kirkham, C., Bertoni, C., Cartwright, J., Lensky, N. G., Sirota, I., Rodriguez, K., & Hodgson, N. (2020). The demise of a 'salt giant' driven by uplift and thermal dissolution. *Earth and Planetary Science Letters*, 531, 115933. <https://doi.org/10.1016/j.epsl.2019.115933>
- Kirkham, C., & Cartwright, J. (2021). Restoration of multi-phase salt tectonic deformation using passive strain markers. *Basin Research*, 33(4), 2453–2473. <https://doi.org/10.1111/bre.12564>
- Kirkham, C., Cartwright, J., Bertoni, C., Rodriguez, K., & Hodgson, N. (2019). 3D kinematics of a thick salt layer during gravity-driven deformation. *Marine and Petroleum Geology*, 110, 434–449. <https://doi.org/10.1016/j.marpetgeo.2019.07.036>
- Kirkham, C., Cartwright, J., Bertoni, C., & van Rensbergen, P. (2020). The genesis of a giant mud canopy by catastrophic failure of a thick evaporite sealing layer. *Geology*, <https://doi.org/10.1130/G47430.1>
- Kirkham, C., Cartwright, J., Hermanrud, C., & Jebsen, C. (2017). The spatial, temporal and volumetric analysis of a large mud volcano province within the Eastern Mediterranean. *Marine and Petroleum Geology*, 81, 1–16. <https://doi.org/10.1016/j.marpetgeo.2016.12.026>
- Kirkham, C., Cartwright, J., Hermanrud, C., & Jebsen, C. (2018a). The formation of giant clastic extrusions at the end of the Messinian salinity crisis. *Earth and Planetary Science Letters*, 482, 434–445. <https://doi.org/10.1016/j.epsl.2017.11.001>
- Kirkham, C., Cartwright, J., Hermanrud, C., & Jebsen, C. (2018b). The genesis of mud volcano conduits through thick evaporite sequences. *Basin Research*, 30, 217–236. <https://doi.org/10.1111/bre.12250>
- Krijgsman, W., Hilgen, F., Raffi, I., Sierro, F., & Wilson, D. (1999). Chronology, causes and progression of the Messinian salinity crisis. *Nature*, 400, 652–655. <https://doi.org/10.1038/23231>
- Letouzey, J., Colletta, B., Vially, R. A., & Chermette, J. (1995). Evolution of salt-related structures in compressional settings. In M. P. A. Jackson, D. G. Roberts, & S. Snelson (Eds.), *Salt tectonics: A global perspective* (Vol. 65, pp. 41–60). AAPG Memoir. <https://doi.org/10.1306/M65604C3>
- Li, S., Abe, S., Reuning, L., Becker, S., Urai, J. L., & Kukla, P. A. (2012). Numerical modelling of the displacement and deformation of embedded rock bodies during salt tectonics: A case study from the South Oman Salt Basin. *Geological Society, London, Special Publications*, 363, 503–520. <https://doi.org/10.1144/SP363.24>
- Lofi, J., Sage, F., Déverchère, J., Loncke, L., Maillard, A., Gaullier, V., Thinon, I., Gillet, H., Guennoc, P., & Gorini, C. (2011). Refining our knowledge of the Messinian salinity crisis records in the offshore domain through multi-site seismic analysis. *Bulletin De La Société Géologique De France*, 182, 163–180. <https://doi.org/10.2113/gssgfbull.182.2.163>
- Loncke, L., Gaullier, V., Mascle, J., Vendeville, B., & Camera, L. (2006). The Nile deep-sea fan: An example of interacting sedimentation, salt tectonics, and inherited subsalt paleotopographic features. *Marine and Petroleum Geology*, 23, 297–315. <https://doi.org/10.1016/j.marpetgeo.2006.01.001>
- Loncke, L., Mascle, J., & Parties, F. S. (2004). Mud volcanoes, gas chimneys, pockmarks and mounds in the Nile deep-sea fan (Eastern Mediterranean): Geophysical evidences. *Marine and Petroleum Geology*, 21, 669–689. <https://doi.org/10.1016/j.marpetgeo.2004.02.004>
- Løseth, H., Wensaas, L., Arntsen, B., Hanken, N.-M., Basire, C., & Graue, K. (2011). 1000 m long gas blow-out pipes. *Marine and Petroleum Geology*, 28, 1047–1060. <https://doi.org/10.1016/j.marpetgeo.2010.10.001>
- Manzi, V., Gennari, R., Hilgen, F., Krijgsman, W., Lugli, S., Roveri, M., & Sierro, F. J. (2013). Age refinement of the Messinian salinity crisis onset in the Mediterranean. *Terra Nova*, 25, 315–322. <https://doi.org/10.1111/ter.12038>
- Mascle, J., Mary, F., Praeg, D., Brosolo, L., Camera, L., Ceramicola, S., & Dupré, S. (2014). Distribution and geological control of mud volcanoes and other fluid/free gas seepage features in the Mediterranean Sea and nearby Gulf of Cadiz. *Geo-Marine Letters*, 34, 89–110. <https://doi.org/10.1007/s00367-014-0356-4>
- Meilijson, A., Hilgen, F., Sepúlveda, J., Steinberg, J., Fairbank, V., Flecker, R., Waldmann, N. D., Spaulding, S. A., Bialik, O. M., Boudinot, F. G., Illner, P., & Makovsky, Y. (2019). Chronology with a pinch of salt: Integrated stratigraphy of Messinian evaporites in the deep Eastern Mediterranean reveals long-lasting halite deposition during Atlantic connectivity. *Earth-Science Reviews*, 194, 374–398. <https://doi.org/10.1016/j.earscirev.2019.05.011>
- Oppo, D., Evans, S., Iacopini, D., Kabir, S. M., Maselli, V., & Jackson, C.-A.-L. (2020). Leaky salt: Pipe trails record the history of cross-evaporite fluid escape in the northern Levant Basin, Eastern Mediterranean. *Basin Research*, 33(3), 1798–1819. <https://doi.org/10.1111/bre.12536>
- Peel, F. J. (2014). The engines of gravity-driven movement on passive margins: Quantifying the relative contribution of spreading vs. gravity sliding mechanisms. *Tectonophysics*, 633, 126–142. <https://doi.org/10.1016/j.tecto.2014.06.023>
- Pichel, L. M., Peel, F., Jackson, C. A., & Huuse, M. (2018). Geometry and kinematics of salt-detached ramp syncline basins. *Journal of Structural Geology*, 115, 208–230. <https://doi.org/10.1016/j.jsg.2018.07.016>
- Pierre, C., Bayon, G., Blanc-Valleron, M.-M., Mascle, J., & Dupré, S. (2014). Authigenic carbonates related to active seepage of methane-rich hot brines at the Cheops mud volcano, Menes caldera (Nile deep-sea fan, eastern Mediterranean Sea). *Geo-Marine Letters*, 34, 253–267. <https://doi.org/10.1016/j.jsg.2018.07.016>
- Prinzhofer, A., & Deville, E. (2013). Origins of hydrocarbon gas seeping out from offshore mud volcanoes in the Nile delta. *Tectonophysics*, 591, 52–61. <https://doi.org/10.1016/j.tecto.2011.06.028>
- Quirk, D. G., Schødt, N., Lassen, B., Ings, S. J., Hsu, D., Hirsch, K. K., & von Nicolai, C. (2012). Salt tectonics on passive margins: Examples from Santos, Campos and Kwanza basins. *Geological Society, London, Special Publications*, 363, 207–244. <https://doi.org/10.1144/SP363.10>

- Rowan, M. G., Peel, F. J., & Vendeville, B. C. (2004). Gravity-driven fold belts on passive margins. *AAPG Memoir*, 82, 157–182. <https://doi.org/10.1306/M82813C9>
- Said, R. (1962). *The geology of Egypt*. Elsevier.
- Salem, R. (1976). Evolution of Eocene-Miocene sedimentation patterns in parts of northern Egypt. *AAPG Bulletin*, 60, 34–64. <https://doi.org/10.1306/83D92280-16C7-11D7-8645000102C1865D>
- Schultz-ELA, D. (2001). Excursus on gravity gliding and gravity spreading. *Journal of Structural Geology*, 23, 725–731. [https://doi.org/10.1016/S0191-8141\(01\)00004-9](https://doi.org/10.1016/S0191-8141(01)00004-9)
- Stewart, S. (2007). Salt tectonics in the North Sea Basin: A structural style template for seismic interpreters. *Special Publication-Geological Society of London*, 272, 361–396. <https://doi.org/10.1144/GSL.SP.2007.272.01.19>
- Stewart, S. A., & Davies, R. J. (2006). Structure and emplacement of mud volcano systems in the South Caspian Basin. *AAPG Bulletin*, 90, 771–786. <https://doi.org/10.1306/11220505045>
- Worrall, D., & Snelson, S. (1989). Evolution of the northern Gulf of Mexico, with emphasis on Cenozoic growth faulting and the role of salt. In A. W. Bally & A. R. Palmer (Eds.), *The geology of North America—An overview* (pp. 97–138). The geology of North America; an overview: Geological Society of America. <https://doi.org/10.1130/DNAG-GNA-A.97>
- Zucker, E., Gvirtzman, Z., Steinberg, J., & Enzel, Y. (2020). Salt tectonics in the Eastern Mediterranean Sea: Where a giant delta meets a salt giant. *Geology*, 48, 134–138. <https://doi.org/10.1130/G47031.1>

How to cite this article: Kirkham, C., & Cartwright, J. (2022). Mud volcanoes and dissolution structures as kinematic markers during salt tectonic deformation. *Basin Research*, 34, 99–120. <https://doi.org/10.1111/bre.12612>